Geomorphology 318 (2018) 354–374

Contents lists available at ScienceDirect

Geomorphology

journal homepage: www.elsevier.com/locate/geomorph

Geochemical composition and provenance of aeolian sands in the Ordos Deserts, northern China

Qianqian Liu [a,b,c], Xiaoping Yang [d,e,*]

[a] Key Laboratory of Cenozoic Geology and Environment, Institute of Geology and Geophysics, Chinese Academy of Sciences, Beijing 100029, China
[b] University of Chinese Academy of Sciences, Beijing 100049, China
[c] Institutions of Earth Science, Chinese Academy of Sciences, China
[d] School of Earth Sciences, Zhejiang University, Hangzhou 310027, China
[e] Geographisches Institut, Universität Heidelberg, Im Neuenheimer Feld 348, 69120 Heidelberg, Germany

ARTICLE INFO

Article history:
Received 23 December 2017
Received in revised form 25 June 2018
Accepted 25 June 2018
Available online 4 July 2018

Keywords:
Aeolian process
Sediment provenance
Trace element
Rare earth element
Fluvial process
Geomorphology

ABSTRACT

Identifying the provenance of aeolian sediments in deserts is of great importance for understanding the Earth surface processes. In this context, we conducted detailed fieldwork in the Ordos Deserts (Maowusu and Kubuqi) in the middle portion of the desert belt in northern China, and measured the major, trace and rare earth elements (REE) of aeolian sands and their potential source rocks and sediments. Our results show that aeolian sands in the eastern (northeastern) and western (southwestern) Maowusu (Mu Us) Sandy Land exhibit different degrees of mineralogical maturity and Eu/Eu* values. Thus, we interpret that these aeolian sands have different provenances, though in the same sandy land. Our data suggest that the local lacustrine sediments and sandstones are the main sources of aeolian sands in the eastern province of the Maowusu Sandy Land, while aeolian sands in the western Maowusu Sandy Land and the Kubuqi Desert have the same external sources. The comparison of geochemical compositions of sediments in the Ordos Deserts with their potential sources in adjacent regions indicates that there is no genetic linkage between the Helan Mountains, the Yinshan Mountains and the Ordos Deserts although they are not far apart. The Qilian Orogenic Belt in the northeastern margin of the Tibetan Plateau is, however, the most likely original provenance for the western Maowusu (Mu Us) Sandy Land and the Kubuqi (Hobq) Desert, but with fluvial sediments in the Ningxia-Inner Mongolian section of the Yellow River as the immediate source. In one side, our results demonstrate that dune fields that are close to each other can have significantly different source sediments. On the other hand, our work suggests that some dune fields and landforms that are far apart from one another, e.g., the Badain Jaran Desert in western Inner Mongolia, the Ordos Deserts and the fluvial sediments in Ningxia-Inner Mongolian section of the Yellow River, can share the same ultimate sources.

1. Introduction

Aeolian deposits are significant components of the Earth's landscapes, and dunefields are common in arid and semi-arid areas (Muhs et al., 1996; Goudie, 2002; Blümel, 2013; Williams, 2014; Muhs, 2017), especially in northwestern China (Zhu et al., 1980; Yang et al., 2012; Dong et al., 2013). Dunes in such areas may record even subtle environmental and climatic changes because ecosystems in arid and semi-arid regions are fragile and can be easily disturbed (Zhu et al., 1980; Li and Yang, 2014), making them sensitive landforms for paleoclimatic studies (Eitel et al., 2005; Thomas and Wiggs, 2008; Chase, 2009; Lancaster et al., 2013; Lehmkuhl et al., 2018). The deserts may impact even the entire Earth system because dust from deserts has a significant influence on radiation balance, biogeochemical cycles, air pollution and human health (Goudie, 2009). Thus, studies of deserts have important implications for not only understanding climatic, environmental changes and Earth surface processes, but also human health and infrastructure.

Provenance of aeolian sands is an indispensable part of desert studies, providing better understanding on the responses of different surface processes to tectonic movement and climatic changes (Sepulchre et al., 2006; Williams, 2014; Yang and Eitel, 2016), and improving interpretation for the climatic signals in aeolian deposits. As rivers also play significant roles in the formation and evolution of landscapes in arid and semi-arid areas, understanding the interactions between aeolian and fluvial processes is critical for reconstructing climatic changes (Nanson et al., 1992; Williams, 1994, 2015; Bullard and McTainsh, 2003; Cohen et al., 2010). Earlier palaeoenvironmental and palaeoclimatic studies

* Corresponding author at: School of Earth Sciences, Zhejiang University, Hangzhou 310027, China.
E-mail address: xpyang@zju.edu.cn (X. Yang).

https://doi.org/10.1016/j.geomorph.2018.06.017
0169-555X/

in arid and semi-arid areas suggest that aeolian processes were predominant during dry and cold climate conditions while paleosols, lacustrine deposits and carbonate in soils generally represent relatively humid and warm epochs (Zhu et al., 1980; Yang et al., 2003, 2013; Bubenzer et al., 2007; Mächtle et al., 2010; Singhvi et al., 2010). In many cases, however, formation of dunes may be controlled by sand supplies (Williams, 1994, 2015; Cohen et al., 2010; Muhs, 2017), and therefore understanding what the sand sources are is crucial.

The Ordos Deserts refer to the deserts located in the Ordos Plateau in the middle portion of the desert belt in northern China, including the Maowusu (Mu Us) Sandy Land and the Kubuqi (Hobq) Sand Sea/Desert (Fig. 1). Some studies have been undertaken to identify the exact sources of aeolian sands in this region. Rao et al. (2011a) proposed that coarse particles in the Ordos Deserts were mainly derived from underlying sandstones and fine particles sourced primarily from the fluvial sediments of the Yellow River. Stevens et al. (2013) suggested that detrital particles carried by the Yellow River from the northern Tibetan Plateau were the ultimate sediment sources of the western Maowusu Sandy Land while weathering sandstones were the primary sources of the eastern Maowusu Sandy Land. However, these previous studies were based on a small quantity of samples, and the regional variation was not thoroughly reflected in the sampling.

Geochemical approaches have been widely used to determine the provenance of wind-blown deposits (Muhs et al., 1996, 2013; Yang et al., 2007a, 2007b, 2008; Yang et al., 2009; Pullen et al., 2011; Rao et al., 2011a, 2011b; Liu and Yang, 2013; Stevens et al., 2013; Lancaster et al., 2015; Hu and Yang, 2016). Sr-Nd isotope compositions (Yang et al., 2009; Rao et al., 2011b), trace and rare earth elements (REE) compositions (Muhs et al., 1996; Yang et al., 2007a, 2007b; Liu and Yang, 2013; Hu and Yang, 2016), mineralogical maturity (Muhs, 2004; Muhs et al., 2013), detrital zircon U-Pb age profiles (Pullen et al., 2011; Stevens et al., 2013), and heavy mineral compositions (Stevens et al., 2013; Lancaster et al., 2015) have all been found to be useful in exploring sources of sediments. To improve our understanding of the provenance of aeolian sediments in the Ordos Deserts and the potential roles of the Yellow River in shaping the landscapes of the Ordos Plateau, we conducted detailed fieldwork in both the Maowusu Sandy Land and the Kubuqi Desert, and collected aeolian sand samples and potential source sediments, with a goal of ascertaining their regional variations. Based on the data of major and trace element compositions, here we aim to clarify the provenance and regional variations of the aeolian sands in the Ordos Deserts, and further to explore the interactions between aeolian processes and the Yellow River in shaping the landforms of the Ordos Deserts.

2. Regional setting

The Ordos Deserts are located in the Ordos Plateau and are bordered by the Yellow River in the west, north and east and by the Loess Plateau in the south. Outside of the region bounded by the Yellow River, the

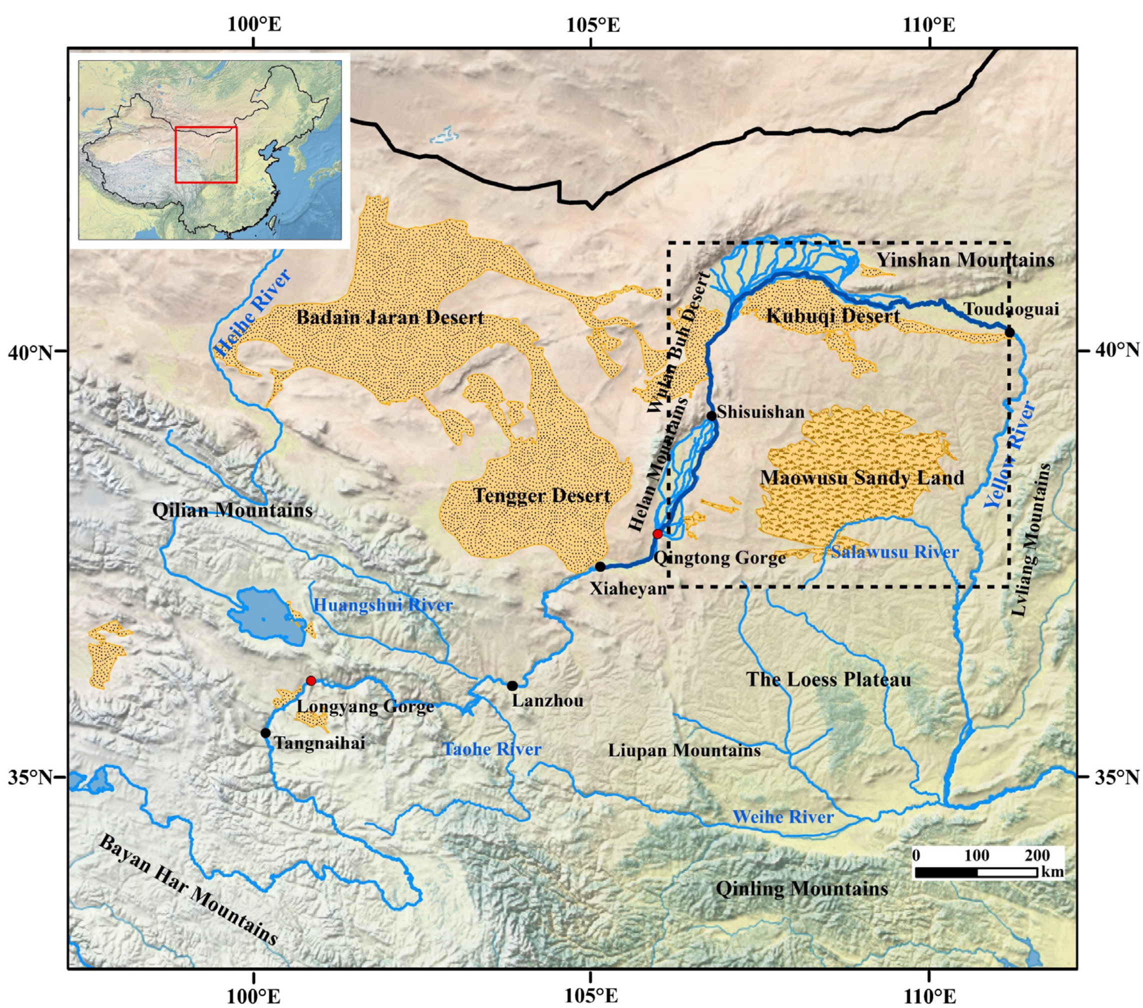

Fig. 1. Location of the study area. The Ordos Deserts refer to the Maowusu Sandy Land and the Kubuqi Desert (The rectangle with black dashed lines marks the location of Fig. 2). The Ningxia-Inner Mongolian section is found mainly along the river course from Qingtong Gorge to Toudaoguai.

Helan Mountains occur to the west, the Yinshan Mountains to the north, and the Lüliang Mountains to the east (Fig. 1). The bedrock of the Ordos Plateau includes Archean and Paleoproterozoic metamorphic crystalline rocks, covered by thick Proterozoic, Paleozoic and Mesozoic sediments. In the desert, loosely cemented and easily weathered Jurassic and Cretaceous sandstones are the most common kinds of rocks. Rocks in the Helan Mountains and the Yinshan Mountains include Archean and Paleo-Proterozoic gneiss, marble, quartzite and granite, and Paleozoic and Mesozoic sandstone, shale and conglomerate. Rocks in the Qilian Mountains include Precambrian basic-ultrabasic volcanic rocks, granites, hypometamorphic and epimetamorphic rocks, Paleozoic and Mesozoic volcanic rocks, clastic sediments, carbonatite and metamorphic rocks (Ma et al., 2004).

Situated in a transitional climatic zone (Fig. 2), the Ordos Deserts show clear regional variations in their geomorphology (Zhu et al., 1980). While active dunes cover most parts of the Kubuqi Desert (Zhu et al., 1980; Yang et al., 2016), fixed (i.e., vegetated) and semi-fixed dunes are the main types of aeolian landforms in the Maowusu Sandy Land (Zhu et al., 1980; Yang et al., 2012). The Maowusu Sandy Land lies in the southeastern part of the Ordos Plateau, with an area of 3.2×10^4 km^2. The mean annual temperature is 6–8°C, and the mean annual precipitation is as high as 440 mm in the east and as low as 250 mm in the west (Fig. 2). The present predominant wind in the sandy land is from northwest to southeast as the resultant drift directions (Fryberger and Dean, 1979) show (Fig. 2). Quaternary aeolian sediments and fluvial and lacustrine deposits make up the main materials of the present surface. In recent decades, great effort has been made to fix mobile dunes in the Maowusu Sandy Land, using aerial seeding and planting grasses and trees with irrigation. Positive effects on desertification control from these efforts are visible. Many seasonal and permanent rivers with headwaters in the Maowusu Sandy Land (Fig. 2) flow southeastwards and are tributaries of the Yellow River (Zhu et al., 1980).

The Kubuqi Desert is about 400 km long from east to west and covers an area of ~1.6×10^4 km^2 (Yang et al., 2012). Its mean annual precipitation ranges from ~150 mm in the west to ~400 mm in the east (Fig. 2). The present predominant wind is from northwest to southeast (Yang et al., 2016; Fig. 2), similar to that in the Maowusu Sandy Land. Ten tributaries originate from the Ordos Plateau and flow across the Kubuqi Desert, from south to north, and finally join the Yellow River (Zhu et al., 1980; Pan et al., 2015; Fig. 2). These tributaries are characterized by high sediment loads, with average annual sediment load of nearly 2×10^7 t (Lin et al., 2014), but average annual runoff has been as low as 1.27 $\times 10^8$ m^3 in the last 60 years (Wu, 2004).

3. Sample selection and analytical methods

We collected 25 aeolian sand samples in the Maowusu Sandy Land, with an effort to sample most of this extensive landscape. Nine sandstone samples from different areas were also collected in the Sandy Land. Among them, three samples were reddish-brown, six were grayish-green. Considering that in the Maowusu Sandy Land there are abundant lake basins, 14 lacustrine sediment samples were collected, 12 of them from a section of a dried lake bed (Fig. 2).

We collected 14 aeolian sand samples in the Kubuqi Desert, all from the top of active dunes, and along the tributaries of the Yellow River. Two sandstone samples were collected in east part of the desert also (Fig. 2).

Recognizing that fine sediment fractions in the Ordos Deserts may have different transport processes and sources than coarse fractions, the fine grain size fraction (<125 μm) were separated from coarse grains by dry sieving. Bulk samples and fine fractions were analyzed for major element abundances with X-ray fluorescence spectrometry (XRF) using a PANalyticle XRF Spectrometer in the Laboratory of Cenozoic Geology and Environment, Institute of Geology and Geophysics, Chinese Academy of Sciences. All samples were first pulverized to powder smaller than 75 μm (Tyler standard 200 mesh), and dried at 100 °C in a dry oven. After this preparation, 0.7 g of sample powder was mixed with 7 g dilithium tetraborate ($Li_2B_4O_7$) flux, and then fused at 1100 °C in a muffle oven. After melting, fluid was poured into a platinum mould to make a fusion glass with a smooth surface, and finally measured with the XRF spectrometer. Loss on Ignition (LOI) was obtained by weighing after 1 h of heating at 900 °C. The LOI and major element concentrations are expressed as wt%, with all the iron expressed as Fe_2O_3. Analytical uncertainties are <±1%.

Trace elements, including the REE were measured using a HR-ICP-MS in the Beijing Research Institute of Uranium Geology, Chinese Ministry for Nuclear Industries. Sample powders (<75 μm) (40 mg) were first dissolved in 1 ml HF and 0.3 ml (1:1) HNO_3, shaken for 15 min with an ultra-sonic device and then heated for 24 h in order to break down silicates and other salts. Then samples were re-dissolved in 1 ml HF, 0.3 ml (1:1) HNO_3 and 0.5 ml $HClO_4$, placed in a capped TEFLON vessel for 7 days in order to further break down silicates, fluorides and zircons. 2 ml (1:1) HNO_3 were further added and dried twice until no remaining residue was detectable. Dissolved samples were diluted to 49 ml with 1 ml 1% HNO_3, and 500 ppb indium was added as an internal standard before the final measurement with the HR-ICP-MS.

The Chemical Index of Alteration (CIA) was defined to quantify the degree of subaerial weathering and measure the degree of weathering and transformation of silicate minerals to secondary clay minerals (e.g., kaolinite, illite and smectite) relative to fresh parent rocks. The calculation equation of the index is: $CIA = [Al_2O_3 / (Al_2O_3 + CaO^* + Na_2O + K_2O)] \times 100$ (in molar proportions). Here CaO^* represents Ca in silicate-bearing minerals only. In our study, carbonate CaO was not distinguished from silicate CaO by experiment, so the method of McLennan (1993) was applied. When the concentration of CaO was less than or equal to the concentration of Na_2O, the CaO value was adopted as the CaO^* value; otherwise the Na_2O value was used for the calculation of CIA.

4. Results

The geochemical compositions of all samples are listed in Table 1.

4.1. Major elements

Compared with bulk samples, the fine sediment fractions have slightly lower SiO_2 content, but obviously higher Fe_2O_3, TiO_2, MnO_2, and MgO contents (Fig. 3), indicating that the fine fractions contain more clay minerals and lower amounts of quartz and feldspars. Almost all samples have a low degree of chemical weathering, with CIA values < 57, except the sandstone samples collected in the Kubuqi Desert, which have an average CIA value of 61.3 (Table 1). In the Maowusu Sandy Land, the bulk aeolian sand samples have slightly higher CIA values than sandstone and lacustrine samples collected nearby, and similar CIA values to the fine particles. In the Kubuqi Desert, sandstone samples have the highest CIA values, while the lowest CIA values occur in the bulk aeolian sand samples (Table 1).

One important characteristic is that the aeolian sand samples collected in the western province of the Maowusu Sandy Land have higher SiO_2 and lower Na_2O and K_2O compared with those collected in the eastern province of the sandy land (Fig. 3).

4.2. Trace elements

The majority of trace elements are depleted compared to UCC in all samples, especially Cd, Tl and Bi. The fine fractions of aeolian sand show slightly higher concentrations of almost all trace elements than the bulk sand samples, especially the elements Sb, Zr and Hf. The lacustrine sediments and sandstone samples from the Maowusu Sandy Land have similar distribution patterns to those of the aeolian sand samples, especially samples collected in the eastern Maowusu Sandy land, with slight differences in concentrations of Cr and Mo. The distribution

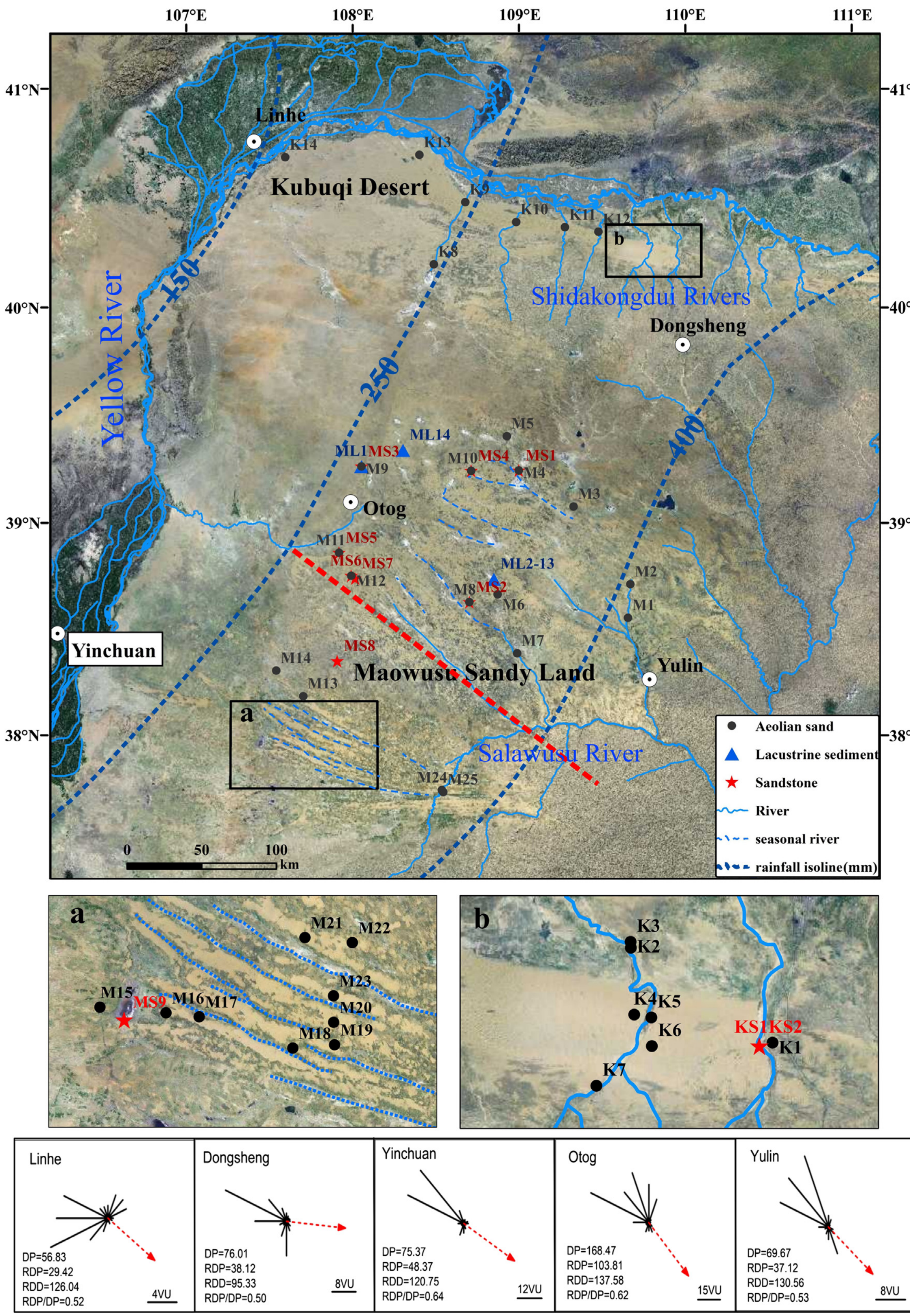

Fig. 2. Distribution of sampling sites. The Maowusu Sandy Land is divided by the dashed red line into two provinces on the basis of major element compositions, i.e., samples M1 to M12 refer to the northeastern province (in the following text and figures as eastern) and samples from M13 to M25 belong to the southwestern province (in the following text and figures as western). Sand roses showing wind strengths and directions are calculated following Fryberger and Dean (1979) with data from the U.S. National Climatic Data Center (NCDC) from 1973 to 2016. DP, Drift Potential; RDP, Resultant Drift Potential; RDP/DP, wind direction variability and RDD, Resultant Drift Direction.

Table 1
Abundances of major elements (%), concentrations of REE and traces elements (ppm) and ratios of elements in the samples of this study.

Samples	M1	M2	M3	M4	M5	M6	M7	M8	M9	M10	M11	M12
SiO_2	74.86	76.82	71.84	75.34	73.02	72.89	75.51	78.28	75.25	74.47	79.63	78.61
Al_2O_3	12.84	12.39	14.03	12.74	12.85	12.80	12.36	11.60	12.23	13.09	10.88	11.46
Fe_2O_3	2.06	1.16	2.87	1.82	3.36	3.43	1.53	1.50	1.42	2.27	1.19	1.05
CaO	1.58	1.44	1.98	1.51	1.68	1.88	2.01	1.24	1.82	1.79	1.16	1.24
MgO	0.54	0.31	0.68	0.47	0.66	0.67	0.60	0.44	0.69	0.61	0.30	0.34
K_2O	2.81	2.72	2.60	2.84	2.57	2.44	2.80	2.86	2.53	2.54	2.74	2.75
Na_2O	3.43	3.44	3.83	3.45	3.43	3.53	3.32	3.13	3.27	3.56	2.91	3.07
TiO_2	0.43	0.20	0.75	0.32	0.73	1.00	0.31	0.22	0.20	0.51	0.09	0.15
MnO	0.04	0.02	0.07	0.03	0.06	0.07	0.03	0.02	0.03	0.05	0.01	0.02
LOI	1.52	1.13	1.44	1.20	1.26	1.20	1.87	1.08	1.62	0.94	0.62	0.76
CIA	52.86	52.67	52.67	52.79	53.11	52.25	50.69	52.72	51.93	52.82	52.66	52.90
Li	8.90	7.81	9.32	10.3	8.19	9.66	9.48	7.98	11.0	15.0	7.14	7.54
Be	1.61	1.72	1.06	1.11	1.41	1.18	1.82	1.35	2.09	1.94	1.37	1.61
Sc	4.49	2.66	6.76	5.73	3.74	6.26	3.81	2.82	3.98	8.12	1.72	2.69
V	33.8	17.5	39.5	55.1	24.7	46.9	30.0	22.4	26.4	49.1	12.1	18.7
Cr	30.8	143	32.9	47.6	122	249	21.4	175	18.6	33.3	319	12.5
Co	3.65	3.41	4.41	5.18	4.04	6.32	3.28	3.99	4.06	7.14	4.24	2.16
Ni	6.83	7.42	6.18	7.50	7.18	10.7	5.75	8.46	7.42	11.8	10.3	3.69
Cu	5.77	4.74	6.78	9.68	6.02	10.0	8.54	6.00	4.83	4.51	3.95	2.74
Zn	21.6	14.6	27.9	29.3	18.3	30.7	18.3	15.6	22.0	31.4	14.1	13.4
Ga	12.9	11.7	13.3	13.5	11.8	13.0	11.7	10.9	12.0	13.6	9.49	10.2
Rb	76.6	73.2	67.5	71.8	74.4	67.3	73.3	75.5	73.3	65.5	73.3	74.4
Sr	383	367	412	378	382	346	343	318	321	309	276	290
Y	10.7	7.55	16.8	14.6	8.60	17.8	9.72	7.68	8.73	14.0	5.37	8.77
Mo	0.563	2.25	0.375	0.376	1.65	3.02	0.356	2.81	0.247	0.309	4.53	0.342
Cd	0.136	0.016	0.131	0.099	0.064	0.107	0.033	0.062	0.045	0.064	0.112	0.044
Sb	0.178	0.150	0.149	0.285	0.162	0.291	0.264	0.175	0.245	0.186	0.166	0.139
Cs	1.90	1.82	1.67	2.03	1.76	2.03	1.88	1.73	2.68	4.01	1.86	1.77
Ba	917	894	857	839	928	765	870	896	767	647	816	817
Tl	0.513	0.493	0.455	0.495	0.506	0.449	0.491	0.488	0.543	0.519	0.490	0.520
Pb	15.5	15.2	15.1	16.4	14.9	16.1	14.9	15.5	17.7	15.3	15.2	14.7
Bi	0.352	0.373	0.217	0.092	0.058	0.108	0.156	0.083	0.066	0.059	0.036	0.046
Th	5.39	2.11	3.34	8.01	2.81	6.63	3.60	2.65	3.47	4.19	2.12	2.37
U	0.951	0.540	0.999	1.70	0.749	1.49	0.875	0.776	1.01	1.84	0.675	0.775
Nb	6.94	3.93	12.8	11.7	5.52	15.4	5.71	4.02	3.90	5.60	2.22	3.78
Ta	0.460	0.289	0.837	0.868	0.388	1.21	0.666	0.279	0.344	0.430	0.167	0.263
Zr	215	119	492	475	129	671	235	161	120	162	76.7	85.3
Hf	5.52	3.02	11.3	11.8	3.24	15.8	5.86	4.05	3.40	4.64	2.13	2.30
La	20.1	12.5	19.8	24.5	16.0	24.2	16.9	14.9	16.3	23.9	11.4	12.3
Ce	37.2	21.3	37.0	47.0	28.0	45.8	30.8	25.9	29.8	44.0	19.5	20.9
Pr	3.95	2.53	4.42	5.59	3.26	5.52	3.63	2.99	3.37	5.15	2.25	2.40
Nd	14.7	9.46	17.0	21.5	12.3	21.1	13.9	11.2	12.6	19.8	8.38	9.01
Sm	2.43	1.62	3.04	3.74	2.02	3.78	2.39	1.86	2.16	3.46	1.42	1.54
Eu	0.693	0.539	0.826	0.783	0.612	0.825	0.674	0.542	0.656	0.890	0.469	0.503
Gd	1.87	1.36	2.58	2.82	1.56	2.98	1.90	1.57	1.83	2.93	1.14	1.31
Tb	0.339	0.222	0.471	0.484	0.271	0.576	0.316	0.252	0.305	0.474	0.170	0.267
Dy	1.83	1.29	2.93	2.65	1.54	3.13	1.87	1.34	1.65	2.62	1.07	1.48
Ho	0.356	0.253	0.563	0.496	0.301	0.624	0.333	0.273	0.303	0.472	0.181	0.274
Er	1.07	0.754	1.76	1.56	0.963	1.82	1.01	0.791	0.881	1.44	0.562	0.902
Tm	0.200	0.131	0.324	0.267	0.164	0.358	0.172	0.150	0.150	0.245	0.092	0.176
Yb	1.32	0.825	2.03	1.90	1.15	2.42	1.22	0.883	1.02	1.54	0.681	1.14
Lu	0.178	0.120	0.282	0.261	0.155	0.328	0.172	0.133	0.144	0.222	0.091	0.148
Eu/Eu*	1.00	1.12	0.91	0.74	1.06	0.76	0.97	0.98	1.01	0.86	1.13	1.09
Th/U	5.67	3.91	3.34	4.71	3.75	4.45	4.11	3.41	3.44	2.28	3.14	3.06
ΣREE	86.2	52.9	93.0	113.6	68.3	113.5	75.3	62.8	71.2	107.1	47.4	52.4
Samples	**M13**	**M14**	**M15**	**M16**	**M17**	**M18**	**M19**	**M20**	**M21**	**M22**	**M23**	**M24**
SiO_2	81.73	81.86	80.90	83.50	82.40	83.48	83.19	85.14	81.11	83.19	84.72	86.39
Al_2O_3	7.88	7.52	8.12	7.54	8.23	7.81	8.11	7.35	8.71	8.61	7.06	6.98
Fe_2O_3	1.70	1.54	1.86	1.35	2.07	1.99	2.21	1.58	2.75	1.42	1.34	1.29
CaO	1.95	2.67	2.08	1.52	1.21	1.00	1.02	0.79	1.28	0.83	0.80	0.74
MgO	0.65	0.59	0.83	0.59	0.79	0.73	0.77	0.60	0.82	0.41	0.52	0.49
K_2O	1.91	1.94	1.96	1.85	1.82	1.65	1.70	1.67	1.80	2.25	1.74	1.73
Na_2O	1.77	1.70	1.74	1.73	1.82	1.71	1.79	1.68	1.95	2.08	1.64	1.57
TiO_2	0.25	0.21	0.28	0.18	0.31	0.29	0.34	0.22	0.45	0.20	0.19	0.18
MnO	0.03	0.04	0.03	0.03	0.04	0.03	0.04	0.03	0.05	0.03	0.02	0.02
LOI	2.04	2.40	2.43	1.81	1.62	1.20	1.48	1.16	1.14	0.94	0.98	1.08
CIA	49.95	49.41	50.84	50.02	53.77	55.20	55.29	55.34	54.12	54.19	54.21	54.87
Li	14.9	11.9	17.5	13.5	15.4	14.4	13.4	12.8	14.8	9.77	11.9	10.3
Be	1.16	1.3	1.25	1.21	0.896	1.30	0.892	1.12	1.55	1.17	1.05	1.12
Sc	4.27	4.02	4.79	3.25	5.26	5.03	5.11	3.88	6.53	3.90	3.36	3.22
V	27.2	24.2	30.1	21.4	40.0	40.2	34.6	28.6	39.2	19.5	22.9	22.3
Cr	25.5	20.6	34.6	17.2	38.3	37.3	46.5	24.7	53.2	15.1	13.9	15.9
Co	4.52	4.02	4.70	3.65	5.03	4.71	4.59	3.79	5.58	2.84	3.51	3.02
Ni	9.11	7.75	10.9	7.85	11.3	10.7	10.1	9.79	10.8	5.12	7.31	7.03

Table 1 (*continued*)

Samples	M13	M14	M15	M16	M17	M18	M19	M20	M21	M22	M23	M24
Cu	7.58	6.53	8.48	6.63	8.28	7.82	7.36	6.73	8.34	4.52	5.99	5.95
Zn	22.1	18.3	25.4	18.8	25.6	23.8	22.6	20.1	26.6	15.3	17.0	15.7
Ga	7.89	7.11	8.44	7.20	8.44	7.75	7.54	6.85	8.79	7.98	6.68	6.30
Rb	65.9	62.4	69.2	64.0	65.1	57.8	55.5	55.6	62.0	67.5	59.2	56.3
Sr	164	174	161	151	150	153	138	132	168	184	138	132
Y	9.59	10.3	10.9	7.67	11.2	9.78	10.0	8.49	14.4	9.92	7.79	6.70
Mo	0.376	0.372	0.381	0.187	0.231	0.209	0.184	0.442	0.332	0.349	0.226	0.205
Cd	0.091	0.045	0.042	0.03	0.075	0.068	0.079	0.039	0.025	0.023	0.079	0.017
Sb	0.555	0.473	0.613	0.567	0.618	0.542	0.610	0.466	0.609	0.318	0.469	0.439
Cs	2.61	2.23	3.03	2.53	2.84	2.37	2.33	2.21	2.46	1.83	2.18	2.03
Ba	516	536	481	483	456	436	403	410	476	629	458	434
Tl	0.449	0.389	0.456	0.366	0.407	0.380	0.344	0.352	0.367	0.428	0.368	0.338
Pb	14.3	13.2	14.1	12.8	14.6	12.8	12.2	11.5	14.1	13.0	11.8	11.0
Bi	0.106	0.097	0.124	0.102	0.126	0.124	0.124	0.811	0.122	0.065	0.079	0.077
Th	4.15	3.60	5.31	3.56	4.76	4.33	4.47	3.51	6.14	3.03	3.08	2.92
U	0.942	0.913	1.24	0.832	1.05	0.945	0.986	0.802	1.21	0.732	0.732	0.680
Nb	5.42	4.43	6.09	4.05	6.48	5.58	6.31	4.32	8.60	4.60	3.77	3.51
Ta	0.422	0.355	0.479	0.385	0.527	0.452	0.484	0.328	0.644	0.307	0.302	0.272
Zr	163	128	205	83.1	150	147	211	93.8	332	173	93.9	101
Hf	4.05	3.34	5.39	2.18	3.96	3.90	5.46	2.44	8.12	4.43	2.51	2.65
La	13.4	12.4	15.5	11.0	14.8	14.6	13.2	10.2	17.9	10.7	9.83	9.12
Ce	24.9	22.5	28.9	20.3	27.7	26.7	24.4	18.8	33.4	18.7	17.7	16.6
Pr	2.83	2.63	3.35	2.32	3.19	3.14	2.83	2.18	3.89	2.24	2.02	1.91
Nd	11.0	10.2	12.9	8.85	12.1	12.0	10.8	8.37	14.8	8.61	7.66	7.25
Sm	2.01	1.94	2.38	1.64	2.24	2.18	1.99	1.56	2.71	1.62	1.44	1.33
Eu	0.501	0.462	0.527	0.417	0.506	0.505	0.456	0.370	0.581	0.435	0.383	0.333
Gd	1.69	1.69	1.98	1.41	1.83	1.91	1.91	1.34	2.44	1.52	1.35	1.08
Tb	0.290	0.315	0.333	0.240	0.352	0.313	0.332	0.255	0.451	0.281	0.225	0.206
Dy	1.68	1.88	1.96	1.42	2.04	1.75	1.73	1.56	2.52	1.72	1.46	1.20
Ho	0.318	0.317	0.368	0.275	0.384	0.342	0.356	0.290	0.495	0.348	0.243	0.227
Er	0.964	1.13	1.19	0.812	1.16	0.995	1.08	0.876	1.58	1.09	0.836	0.707
Tm	0.171	0.179	0.193	0.133	0.217	0.190	0.179	0.156	0.292	0.190	0.154	0.125
Yb	1.14	1.20	1.33	0.894	1.31	1.21	1.27	0.905	1.82	1.32	0.813	0.867
Lu	0.157	0.162	0.184	0.126	0.200	0.193	0.171	0.132	0.275	0.182	0.136	0.120
Eu/Eu*	0.84	0.78	0.75	0.84	0.77	0.76	0.72	0.79	0.69	0.85	0.84	0.85
Th/U	4.41	3.94	4.28	4.28	4.53	4.58	4.53	4.38	5.07	4.14	4.21	4.29
ΣREE	61.1	57.0	71.1	49.8	68.0	66.0	60.7	47.0	83.2	49.0	44.3	41.1

Samples	M25	MS1	MS2	MS3	MS4	MS5	MS6	MS7	MS8	MS9	MF1	MF2
SiO_2	88.61	61.65	70.41	67.32	72.44	77.03	73.97	76.42	69.26	60.25	70.19	71.38
Al_2O_3	5.94	12.64	13.06	12.97	13.83	11.76	12.87	11.51	12.17	13.79	11.60	12.62
Fe_2O_3	0.95	2.71	1.95	2.75	1.88	2.12	2.26	1.66	2.89	6.02	6.27	3.58
CaO	0.58	7.62	3.42	4.64	1.38	1.43	2.22	1.57	4.00	2.29	1.90	2.00
MgO	0.38	1.92	1.07	1.54	1.00	0.48	1.05	0.90	1.51	3.92	1.18	0.99
K_2O	1.63	3.31	3.27	2.19	3.61	2.60	2.29	2.61	2.36	3.01	2.12	2.19
Na_2O	1.50	3.17	3.53	3.17	3.54	3.15	3.37	2.93	2.93	3.86	2.83	3.23
TiO_2	0.13	0.27	0.23	0.33	0.17	0.44	0.32	0.19	0.48	0.63	1.42	1.43
MnO	0.01	0.09	0.03	0.07	0.02	0.05	0.04	0.01	0.08	0.06	0.10	0.09
LOI	0.84	6.93	3.45	4.53	1.94	0.90	1.63	1.76	3.96	6.54	1.54	1.50
CIA	53.15	47.41	46.27	50.32	53.37	52.86	52.02	52.64	49.94	50.65	53.34	53.48
Li	10.4	20.5	11.6	9.96	10.7	7.52	10.7	12.5	17.6	59.7	13.9	13.3
Be	0.756	1.34	1.41	1.63	1.79	1.39	1.55	1.30	2.18	2.53	1.79	1.68
Sc	2.50	4.92	3.81	5.12	3.68	4.33	6.32	3.44	7.99	11.2	10.8	10.1
V	18.2	34.7	32.6	38.0	24.2	27.8	32.7	24.6	43.1	68.5	108	55.9
Cr	8.71	93.3	143	28.6	130	18.6	150	175	194	126	98.9	63.5
Co	2.18	8.57	6.00	4.31	6.41	3.17	6.52	4.92	7.80	18.7	8.79	6.59
Ni	4.95	16.4	10.3	6.22	11.2	4.14	10.8	10.4	13.0	31.0	14.3	11.1
Cu	5.00	7.57	7.36	5.08	5.87	4.10	4.95	4.87	8.68	19.5	11.9	10.9
Zn	12.7	36.4	22.6	23.7	21.7	18.2	21.7	18.7	28.4	101	48.7	41.0
Ga	5.46	14.9	13.2	13.1	13.7	10.6	12.4	11.0	12.7	18.9	14.1	12.8
Rb	53.0	94.5	79.6	70.0	86.4	69.8	60.9	68.5	66.7	132	63.8	63.1
Sr	118	386	396	369	418	292	356	278	304	169	265	292
Y	5.48	11.1	8.89	13.3	7.07	12.6	11.8	8.62	20.0	22.2	25.3	25.1
Mo	0.108	1.19	2.11	0.243	2.55	0.255	2.38	2.99	2.78	1.78	0.487	0.380
Cd	0.033	0.029	0.061	0.094	0.041	0.090	0.088	0.034	0.190	0.043	0.147	0.071
Sb	0.414	0.120	0.162	0.141	0.139	0.167	0.168	0.170	0.276	0.613	0.396	0.295
Cs	1.72	2.87	1.01	2.03	1.32	1.79	1.98	1.90	2.24	12.9	2.58	2.45
Ba	429	1045	1086	799	1224	771	738	759	694	623	559	621
Tl	0.323	0.542	0.485	0.505	0.794	0.421	0.433	0.433	0.420	0.679	0.418	0.366
Pb	9.91	14.7	15.7	16.1	16.1	14.4	15.2	15.0	21.1	20.6	16.3	14.3
Bi	0.064	0.049	0.085	0.058	0.026	0.041	0.050	0.048	0.101	0.210	0.114	0.100
Th	2.55	2.58	3.24	4.50	2.57	4.17	4.30	2.79	6.07	10.2	14.6	9.75
U	0.695	0.749	0.755	1.26	1.56	1.19	1.07	0.797	2.54	2.40	2.94	2.08
Nb	2.88	5.60	4.31	7.99	3.70	8.46	4.80	4.04	8.91	15.2	18.7	14.5
Ta	0.224	0.332	0.269	0.562	0.246	0.658	0.358	0.242	0.599	1.05	0.992	0.600

(*continued on next page*)

Table 1 (*continued*)

Samples	M25	MS1	MS2	MS3	MS4	MS5	MS6	MS7	MS8	MS9	MF1	MF2
Zr	69.6	105	170	359	121	296	168	125	255	240	1189	1309
Hf	1.92	2.77	4.38	8.95	3.16	7.41	4.29	3.24	6.57	6.85	28.6	31.5
La	7.91	21.1	19.7	21.8	22.0	17.7	20.6	14.3	27.8	32.3	46.7	36.6
Ce	14.2	36.4	34.4	40.2	38.0	31.6	38.6	24.6	52.3	61.1	87.9	70.0
Pr	1.63	4.34	3.97	4.70	4.31	3.70	4.60	2.99	6.36	7.18	10.4	8.35
Nd	6.18	16.5	15.0	17.7	15.9	14.0	17.9	11.4	25.0	27.5	39.4	32.1
Sm	1.11	2.81	2.46	2.99	2.52	2.40	3.17	2.02	4.53	4.94	6.46	5.60
Eu	0.290	0.887	0.789	0.766	0.841	0.608	0.836	0.651	1.02	0.935	0.996	1.07
Gd	0.909	2.29	1.84	2.45	1.85	2.01	2.63	1.72	3.99	4.26	4.89	4.32
Tb	0.170	0.370	0.328	0.440	0.278	0.375	0.419	0.291	0.659	0.740	0.877	0.762
Dy	0.909	1.89	1.59	2.38	1.42	2.24	2.24	1.60	3.64	3.98	4.56	4.35
Ho	0.178	0.340	0.309	0.489	0.249	0.415	0.418	0.293	0.683	0.766	0.920	0.873
Er	0.573	1.05	0.840	1.38	0.729	1.34	1.21	0.872	2.02	2.29	2.65	2.50
Tm	0.106	0.169	0.148	0.265	0.116	0.242	0.193	0.149	0.322	0.406	0.457	0.443
Yb	0.709	1.03	0.914	1.68	0.799	1.72	1.38	0.908	2.17	2.46	3.01	2.89
Lu	0.093	0.139	0.130	0.253	0.105	0.231	0.185	0.127	0.300	0.332	0.486	0.469
Eu/Eu*	0.89	1.07	1.14	0.87	1.20	0.85	0.89	1.07	0.74	0.63	0.54	0.67
Th/U	3.67	3.44	4.29	3.57	1.65	3.50	4.02	3.50	2.39	4.25	4.97	4.69
ΣREE	35.0	89.3	82.4	97.5	89.1	78.6	94.4	61.9	130.8	149.2	209.7	170.3

Samples	MF3	MF4	MF5	MF6	MF7	MF8	MF9	MF10	MF11	MF12	MF13	MF14
SiO_2	59.06	69.75	63.16	57.88	71.28	66.26	71.81	66.52	70.58	58.03	70.77	64.81
Al_2O_3	12.51	11.58	10.09	11.29	11.88	12.33	11.76	12.34	12.96	10.53	9.72	9.55
Fe_2O_3	11.17	6.66	13.51	12.60	3.54	7.58	2.81	7.45	3.85	15.68	4.10	6.50
CaO	2.97	1.93	1.91	3.31	2.78	2.27	2.92	2.42	2.22	2.67	4.63	6.64
MgO	1.74	1.20	1.31	1.55	1.12	1.37	1.25	1.41	1.45	1.86	1.32	1.66
K_2O	1.85	2.12	1.75	1.78	2.29	2.29	2.11	2.00	2.24	1.61	1.83	1.71
Na_2O	3.04	2.78	2.32	2.67	3.05	3.07	2.81	3.09	3.16	2.24	2.07	1.84
TiO_2	4.37	1.51	3.08	4.69	0.92	1.89	0.47	2.08	0.79	4.08	0.76	1.17
MnO	0.26	0.11	0.21	0.28	0.07	0.12	0.06	0.14	0.07	0.28	0.09	0.13
LOI	1.46	1.48	1.39	2.16	2.34	1.70	2.99	1.49	2.71	1.22	4.54	5.51
CIA	51.10	53.42	53.41	51.30	49.27	52.33	50.48	52.55	53.20	53.60	52.49	54.70
Li	15.5	14.4	15.4	15.7	13.7	14.3	17.0	14.2	16.0	15.7	20.0	20.0
Be	1.81	1.58	1.23	1.96	1.87	1.47	1.72	1.62	1.72	1.86	2.04	1.57
Sc	21.5	11.3	16.7	22.5	9.10	13.3	8.13	13.8	10.0	26.0	10.2	13.7
V	188	108	287	249	72.7	152	56.1	147	74.9	308	75.5	119
Cr	153	105	235	221	67.7	121	49.4	127	66.2	290	112	218
Co	14.5	9.12	14.4	14.8	6.56	9.76	7.18	10.3	8.22	17.5	9.04	11.8
Ni	18.1	14.0	20.6	19.5	14.4	15.5	15.4	15.5	14.7	22.6	20.1	24.9
Cu	26.5	12.6	22.9	29.4	9.74	14.2	9.24	14.0	10.2	26.3	14.8	18.6
Zn	101	49.8	83.5	107	37.3	56.1	35.4	67.6	47.0	105	44.9	57.4
Ga	17.8	14.1	17.8	19.3	13.0	15.6	12.5	15.8	13.7	21.4	11.2	12.7
Rb	54.0	63.0	54.9	56.0	67.7	64.7	66.5	58.0	68.2	52.3	64.9	60.1
Sr	307	258	210	270	287	284	249	298	286	204	210	225
Y	59.3	27.6	45.9	61.0	21.9	33.3	15.4	34.0	20.1	71.6	22.5	34.4
Mo	1.14	0.617	1.17	1.47	0.821	0.737	0.599	0.610	0.507	1.72	0.604	0.851
Cd	0.272	0.105	0.160	0.291	0.044	0.199	0.093	0.166	0.153	0.524	0.142	0.149
Sb	0.355	0.434	0.743	0.433	0.328	0.257	0.413	0.248	0.393	0.574	1.02	1.30
Cs	2.21	2.58	2.45	2.56	2.57	2.39	3.34	2.29	3.44	2.55	3.19	3.12
Ba	546	566	453	503	635	636	523	588	609	433	458	419
Tl	0.327	0.424	0.302	0.314	0.408	0.390	0.380	0.393	0.519	0.313	0.409	0.375
Pb	17.5	15.7	19.9	19.5	14.5	17.9	15.2	15.1	16.4	19.1	16.6	20.0
Bi	0.147	0.133	0.253	0.166	0.104	0.117	0.099	0.111	0.110	0.245	0.226	0.284
Th	25.6	16.0	30.8	32.4	8.26	17.9	6.03	16.6	5.92	41.3	7.99	19.0
U	5.29	3.04	6.13	6.64	1.85	3.27	1.56	3.32	1.94	8.46	1.88	3.85
Nb	59.9	17.3	45.6	68.7	14.8	10.6	8.11	6.47	12.2	59.8	14.8	21.2
Ta	4.61	0.713	3.46	4.71	1.05	0.442	0.605	0.078	0.776	5.44	1.30	1.49
Zr	2942	1278	2515	4236	733	1628	258	1442	459	4549	654	1568
Hf	67.6	29.7	59.3	97.7	18.2	37.8	6.85	34.4	10.9	102	15.0	38.5
La	81.8	50.4	93.5	103	30.5	56.1	21.9	58.5	25.9	120	27.4	55.5
Ce	157	94.7	177	197	57.9	108	42.5	113	48.9	233	51.5	107
Pr	18.7	11.1	20.5	23.3	6.92	12.8	4.9	13.2	5.79	27.9	6.08	12.8
Nd	70.0	41.7	75.6	87.2	27.1	49.3	18.8	50.4	22.4	105	23.7	49.0
Sm	11.6	6.80	12.0	14.4	4.70	7.94	3.41	8.42	4.21	17.9	4.48	8.83
Eu	1.45	1.11	1.39	1.79	0.962	1.33	0.853	1.24	0.935	1.85	0.901	1.20
Gd	9.75	5.13	8.67	11.7	4.03	6.08	3.00	6.56	3.47	14.1	3.88	7.05
Tb	1.67	0.910	1.44	1.92	0.698	1.09	0.546	1.10	0.691	2.44	0.722	1.26
Dy	8.95	4.93	7.12	10.7	3.56	5.51	2.73	5.46	3.37	11.9	3.66	6.02
Ho	1.69	1.03	1.49	2.13	0.729	1.12	0.549	1.15	0.715	2.57	0.758	1.22
Er	5.48	2.78	4.35	6.45	2.20	3.36	1.52	3.41	2.06	7.40	2.14	3.66
Tm	1.01	0.469	0.790	1.13	0.387	0.576	0.259	0.606	0.360	1.37	0.347	0.623
Yb	6.08	2.89	5.18	7.24	2.28	3.69	1.56	3.56	2.26	8.56	2.20	3.93
Lu	1.01	0.476	0.812	1.12	0.350	0.550	0.278	0.605	0.323	1.34	0.347	0.599
Eu/Eu*	0.42	0.58	0.42	0.42	0.68	0.59	0.82	0.51	0.75	0.36	0.66	0.47
Th/U	4.84	5.26	5.02	4.88	4.46	5.47	3.87	5.00	3.05	4.88	4.25	4.94
ΣREE	376.2	224.4	409.8	469.1	142.3	257.4	102.8	267.2	121.4	555.3	128.1	258.7

Table 1 (*continued*)

Samples	MF3	MF4	MF5	MF6	MF7	MF8	MF9	MF10	MF11	MF12	MF13	MF14
Samples	MF15	MF16	MF17	MF18	MF19	MF20	MF21	MF22	MF23	MF24	MF25	ML1
SiO_2	73.39	71.46	69.25	68.39	71.18	73.66	67.21	73.77	68.25	76.70	78.34	67.07
Al_2O_3	9.86	9.53	10.05	10.24	10.29	10.32	10.11	10.39	10.14	9.71	9.53	11.95
Fe_2O_3	3.09	3.75	6.49	9.10	6.71	5.07	8.94	5.29	8.55	3.46	2.85	2.19
CaO	3.42	4.28	3.31	2.25	2.01	1.62	2.98	1.67	2.61	1.71	1.72	5.66
MgO	1.39	1.40	1.64	1.89	1.66	1.48	1.66	1.29	1.58	1.24	1.16	1.13
K_2O	2.06	1.85	1.79	1.70	1.78	1.85	1.70	1.90	1.73	1.93	1.97	2.39
Na_2O	2.08	1.98	1.94	1.90	2.00	2.06	1.94	2.23	2.01	2.08	2.06	2.95
TiO_2	0.53	0.67	1.23	1.62	1.26	0.91	1.72	1.17	1.57	0.63	0.52	0.24
MnO	0.05	0.08	0.12	0.16	0.12	0.09	0.15	0.10	0.14	0.06	0.05	0.08
LOI	3.95	3.94	3.41	1.86	1.82	1.96	2.71	1.65	2.55	2.01	1.95	5.57
CIA	52.06	52.79	54.69	55.85	54.73	55.80	55.13	54.92	54.43	53.32	52.71	49.28
Li	20.5	20.2	18.9	20.0	21.2	22.9	23.7	21.7	22.2	19.1	17.9	12.4
Be	1.16	1.66	1.35	1.47	1.72	1.32	1.39	1.52	1.98	1.69	1.16	1.34
Sc	8.99	9.98	14.1	18.8	15.9	12.4	18.4	14.2	17.6	9.23	8.06	4.99
V	62.1	71.6	124	174	134	97.1	174	107	168	69.6	56.2	34.6
Cr	72.6	106	257	404	281	154	382	174	373	105	82.5	176
Co	7.51	8.59	11.9	14.3	12.2	10.1	14.4	9.88	13.5	7.43	6.64	6.70
Ni	19.1	20.7	26.1	30.9	27.2	24.3	30.8	20.4	28.1	18.8	17.5	13.6
Cu	13.7	14.6	18.5	19.7	18.4	15.6	21.6	16.0	20.6	12.4	11.7	5.23
Zn	40.5	41.6	61.2	68.5	62.2	53.7	74.0	56.6	70.2	40.3	36.2	25.1
Ga	11.1	11.1	13.1	13.8	13.7	12.3	15.5	13.7	15.1	11.0	10.2	12.0
Rb	72.0	65.7	65.1	59.2	66.0	67.4	63.2	69.7	63.5	67.6	67.8	67.1
Sr	184	202	182	163	169	162	180	186	177	167	173	289
Y	19.9	20.0	33.1	40.5	30.8	25.6	44.2	33.9	43.4	18.2	15.2	12.5
Mo	0.555	0.497	0.924	1.02	0.774	0.885	2.00	0.701	1.35	0.456	0.555	2.40
Cd	0.111	0.042	0.096	0.248	0.070	0.109	0.181	0.204	0.130	0.085	0.043	0.133
Sb	0.829	0.874	1.41	1.37	1.49	1.08	1.20	1.04	1.34	0.747	0.775	0.145
Cs	3.68	3.14	3.46	3.03	3.37	3.40	3.31	3.38	3.24	3.05	2.98	3.68
Ba	467	453	428	391	432	444	396	475	418	435	469	687
Tl	0.422	0.387	0.308	0.347	0.362	0.406	0.399	0.367	0.354	0.370	0.385	0.528
Pb	15.3	16.0	20.8	21.8	19.0	17.4	23.1	18.6	23.2	14.4	13.1	15.0
Bi	0.177	0.200	0.339	0.405	0.310	0.269	0.388	0.241	0.406	0.157	0.141	0.049
Th	10.5	7.86	14.4	14.2	11.0	9.15	21.7	13.1	20.1	6.33	5.24	3.67
U	2.14	1.73	3.15	3.65	2.87	2.38	4.73	2.97	4.37	1.59	1.45	1.44
Nb	11.3	14.0	24.6	30.1	21.6	18.1	17.4	23.7	28.6	11.9	10.2	4.49
Ta	0.754	1.17	2.07	2.11	1.46	1.46	0.414	1.77	2.08	0.992	0.767	0.308
Zr	458	376	1126	2131	1442	873	2374	1208	2043	211	155	113
Hf	10.9	9.31	27.0	49.2	31.3	20.0	53.3	28.3	47.8	5.86	3.92	3.20
La	29.9	27.5	42.4	41.5	34.2	28.2	63.2	40.3	59.5	20.7	18.4	21.3
Ce	57.0	51.3	81.7	79.5	65.6	54.3	122	78.0	115	39.1	35.1	38.1
Pr	6.67	6.03	9.65	9.63	7.90	6.38	14.6	9.43	13.5	4.67	4.13	4.45
Nd	25.6	22.9	37.5	36.9	30.3	24.4	56.4	37.1	51.4	17.7	15.7	17.0
Sm	4.70	4.12	6.95	7.01	5.70	4.61	9.98	6.87	9.46	3.38	2.91	2.95
Eu	0.776	0.799	1.06	1.19	1.04	0.942	1.26	1.03	1.07	0.703	0.651	0.780
Gd	3.84	3.62	5.39	6.17	5.08	4.20	8.08	5.71	7.58	2.87	2.52	2.43
Tb	0.709	0.614	1.06	1.23	0.915	0.818	1.46	1.04	1.44	0.539	0.464	0.403
Dy	3.74	3.32	5.42	6.38	5.17	4.49	7.23	5.54	6.69	3.02	2.35	2.33
Ho	0.737	0.664	1.12	1.30	1.12	0.975	1.51	1.11	1.44	0.607	0.464	0.431
Er	2.10	1.96	3.17	4.07	3.24	2.60	4.47	3.19	4.31	1.81	1.49	1.22
Tm	0.361	0.353	0.631	0.788	0.584	0.492	0.794	0.650	0.808	0.318	0.257	0.225
Yb	2.13	2.14	3.96	5.17	3.82	3.36	5.20	3.86	4.91	2.01	1.56	1.42
Lu	0.320	0.308	0.550	0.704	0.562	0.422	0.810	0.546	0.712	0.316	0.211	0.207
Eu/Eu*	0.56	0.64	0.53	0.56	0.59	0.66	0.43	0.51	0.39	0.69	0.74	0.90
Th/U	4.91	4.54	4.57	3.89	3.83	3.84	4.59	4.41	4.60	3.98	3.61	2.55
ΣREE	138.6	125.6	200.6	201.5	165.2	136.2	297.0	194.4	277.8	97.7	86.2	93.2
Samples	ML2	ML3	ML4	ML5	ML6	ML7	ML8	ML9	ML10	ML11	ML12	ML13
SiO_2	64.76	72.69	69.13	71.23	66.94	72.55	68.06	74.50	72.75	76.65	70.98	77.20
Al_2O_3	10.84	11.60	11.20	11.30	10.88	12.10	10.81	11.40	12.00	11.61	11.70	11.50
Fe_2O_3	1.76	1.17	1.37	1.24	1.57	1.02	1.52	1.07	1.36	0.85	1.53	1.07
CaO	5.31	3.15	4.05	3.40	4.83	3.14	4.55	2.89	3.04	2.06	3.79	2.13
MgO	3.69	1.29	2.49	1.86	3.23	1.16	2.81	1.38	1.17	0.59	2.05	0.56
K_2O	2.59	2.76	2.70	2.78	2.61	2.81	2.59	2.85	2.88	2.91	2.73	2.96
Na_2O	2.92	3.28	3.13	3.15	2.97	3.44	2.95	3.21	3.40	3.30	3.25	3.25
TiO_2	0.26	0.24	0.25	0.19	0.22	0.18	0.22	0.21	0.25	0.18	0.29	0.15
MnO	0.04	0.03	0.03	0.02	0.03	0.03	0.03	0.02	0.03	0.02	0.03	0.02
LOI	7.37	3.11	4.83	3.73	6.24	3.07	5.70	2.90	2.31	1.35	3.68	1.54
CIA	46.61	45.69	45.85	45.78	46.33	45.85	46.34	45.80	46.00	48.72	46.14	48.28
Li	17.7	10.6	15.2	12.0	17.4	10.5	16.7	10.7	10.9	7.15	13.4	8.19
Be	1.04	1.19	1.41	1.09	1.42	1.75	1.55	1.43	1.47	1.38	1.09	1.12
Sc	3.61	2.80	3.33	2.64	3.20	2.69	3.31	2.52	2.99	1.83	3.31	1.93
V	27.8	19.9	27.5	22.6	28.1	18.2	28.9	25.5	27.1	15.5	27.8	15.6

(continued on next page)

Table 1 (*continued*)

Samples	ML2	ML3	ML4	ML5	ML6	ML7	ML8	ML9	ML10	ML11	ML12	ML13
Cr	165	15.1	18.4	94.8	162	22.3	165	13.7	171	8.60	122	142
Co	4.50	2.66	3.17	3.43	4.39	2.68	4.40	2.37	3.59	1.68	3.96	3.52
Ni	10.1	5.23	6.36	7.66	9.75	11.6	12.2	4.51	7.43	3.02	8.24	7.89
Cu	6.14	3.86	4.57	4.23	5.56	3.43	6.17	3.62	4.16	2.35	4.77	3.45
Zn	20.9	18.8	17.0	14.2	18.4	13.7	19.5	15.5	15.5	9.81	18.0	11.3
Ga	10.0	10.8	10.5	10.2	10.3	10.4	10.4	10.4	10.9	9.55	10.8	10.2
Rb	64.8	71.8	69.0	70.4	67.5	68.7	68.3	72.6	73.5	69.3	69.7	74.5
Sr	486	388	431	420	465	387	444	382	390	347	424	343
Y	9.54	8.44	8.60	7.32	8.65	8.39	8.40	7.76	8.68	6.94	9.42	6.32
Mo	1.63	0.196	0.196	1.80	1.96	1.55	1.91	0.153	2.05	0.246	1.37	3.08
Cd	0.089	0.059	0.039	0.029	0.049	0.053	0.066	0.048	0.036	0.035	0.063	0.031
Sb	0.168	0.144	0.170	0.115	0.187	0.097	0.184	0.116	0.161	0.090	0.162	0.115
Cs	1.98	1.61	1.76	1.64	1.90	1.55	1.87	1.58	1.59	1.36	1.74	1.49
Ba	747	886	818	861	783	884	808	878	898	900	847	896
Tl	0.392	0.440	0.380	0.412	0.409	0.494	0.419	0.468	0.420	0.433	0.381	0.483
Pb	12.3	13.4	13.1	13.3	13.0	12.4	12.5	13.6	13.7	12.6	13.1	13.4
Bi	0.053	0.047	0.041	0.038	0.049	0.031	0.056	0.039	0.031	0.023	0.042	0.026
Th	3.71	2.60	2.80	2.23	3.60	2.25	2.48	2.13	2.11	2.04	2.91	1.76
U	1.04	0.754	0.973	0.768	1.09	0.656	1.04	0.767	0.738	0.589	0.968	0.546
Nb	4.96	4.50	4.32	3.70	4.11	3.45	4.01	4.04	4.62	2.94	4.96	3.21
Ta	0.325	0.285	0.283	0.231	0.273	0.225	0.259	0.281	0.327	0.243	0.338	0.234
Zr	206	172	185	157	149	107	165	163	175	162	210	110
Hf	5.16	4.26	4.76	4.06	3.75	2.73	4.18	4.14	4.52	3.85	5.06	2.81
La	17.8	15.1	15.2	13.4	17.3	14.0	14.8	13.3	13.8	12.6	15.6	11.5
Ce	31.3	26.8	27.2	23.6	31.5	24.1	26.2	23.5	24.3	21.7	27.8	19.7
Pr	3.66	3.11	3.18	2.72	3.76	2.83	3.10	2.77	2.88	2.55	3.28	2.28
Nd	13.8	11.9	12.2	10.4	14.5	10.7	11.9	10.5	11.0	9.64	12.7	8.62
Sm	2.37	2.02	2.12	1.77	2.41	1.86	2.06	1.81	1.93	1.64	2.23	1.44
Eu	0.636	0.607	0.619	0.527	0.576	0.564	0.578	0.532	0.606	0.496	0.641	0.499
Gd	2.09	1.73	1.74	1.55	1.94	1.65	1.65	1.58	1.61	1.26	1.95	1.25
Tb	0.303	0.269	0.273	0.248	0.303	0.253	0.281	0.244	0.273	0.212	0.305	0.222
Dy	1.89	1.48	1.53	1.28	1.50	1.37	1.60	1.36	1.58	1.22	1.65	1.13
Ho	0.313	0.293	0.290	0.242	0.272	0.288	0.308	0.264	0.321	0.223	0.308	0.213
Er	1.01	0.898	0.909	0.742	0.853	0.817	0.842	0.765	0.961	0.724	0.990	0.631
Tm	0.175	0.144	0.166	0.133	0.162	0.154	0.151	0.139	0.162	0.121	0.157	0.122
Yb	1.09	0.982	1.08	0.817	0.919	0.820	1.02	0.999	1.04	0.749	1.13	0.706
Lu	0.153	0.131	0.146	0.133	0.147	0.125	0.140	0.111	0.160	0.115	0.153	0.100
Eu/Eu*	0.88	1.00	0.99	0.98	0.82	0.99	0.96	0.97	1.06	1.06	0.94	1.14
Th/U	3.57	3.45	2.88	2.90	3.30	3.43	2.38	2.78	2.86	3.46	3.01	3.22
ΣREE	76.6	65.5	66.7	57.6	76.1	59.5	64.6	57.9	60.6	53.3	68.9	48.4

Samples	ML14	K1	K2	K3	K4	K5	K6	K7	K8	K9	K10	K11
SiO_2	61.63	78.02	74.73	77.75	80.20	80.73	80.32	78.76	76.66	80.23	82.64	82.23
Al_2O_3	11.41	9.05	9.26	9.10	8.85	8.28	8.51	8.92	9.23	8.46	7.89	8.13
Fe_2O_3	3.53	2.29	2.33	2.02	2.03	1.79	1.72	2.02	2.41	2.07	1.59	1.75
CaO	5.06	2.18	3.89	2.81	2.25	1.98	2.11	2.08	2.55	2.12	1.24	1.45
MgO	5.07	0.87	1.04	0.72	0.76	0.69	0.68	0.76	0.96	0.82	0.61	0.69
K_2O	2.39	1.96	2.00	2.28	2.02	1.93	1.99	2.02	2.01	1.88	1.83	1.89
Na_2O	2.45	1.98	2.05	2.14	2.02	1.89	1.98	1.99	2.03	1.84	1.80	1.85
TiO_2	0.41	0.39	0.41	0.36	0.34	0.26	0.26	0.32	0.39	0.30	0.21	0.24
MnO	0.07	0.04	0.04	0.04	0.04	0.03	0.04	0.04	0.04	0.04	0.03	0.03
LOI	8.03	2.38	3.76	2.50	2.25	1.93	2.02	2.32	2.75	2.20	1.59	1.60
CIA	51.71	51.15	50.95	48.88	50.03	49.90	49.52	50.51	51.02	51.10	52.65	51.63
Li	34.9	18.5	18.1	12.4	15.8	14.2	14.9	16.2	16.2	16.6	13.7	14.0
Be	1.56	1.13	1.23	1.14	1.49	1.07	1.28	1.64	1.27	1.49	1.26	1.33
Sc	7.75	5.49	6.28	5.08	5.19	4.31	4.48	5.24	5.64	4.97	4.26	4.30
V	58.8	45.1	43.4	34.9	32.4	28.2	28.5	33.5	34.9	41.6	33.2	28.7
Cr	169	43.3	42.1	26.6	32.4	21.1	17.4	31.1	40.0	40.0	24.2	25.1
Co	10.1	5.43	6.41	4.85	5.66	4.33	4.65	5.41	5.39	5.23	4.48	4.69
Ni	20.7	12.4	14.4	13.6	11.1	9.27	9.70	14.2	12.1	10.9	9.34	9.76
Cu	13.5	8.76	14.2	7.59	8.72	7.17	7.39	8.60	8.89	7.97	6.92	7.28
Zn	45.2	27.9	32.0	23.8	26.0	22.2	22.2	26.9	29.9	24.5	19.8	23.1
Ga	12.6	9.02	9.84	9.20	8.95	7.75	8.06	9.06	9.12	8.35	7.30	7.71
Rb	72.0	67.9	71.9	74.0	74.4	64.6	68.4	72.8	69.9	69.2	64.3	65.2
Sr	476	169	212	227	189	166	183	183	176	168	149	156
Y	14.5	12.1	15.3	12.5	12.1	9.27	9.97	11.4	12.8	11.2	8.74	8.98
Mo	1.66	0.384	0.327	0.422	0.168	0.149	0.233	0.853	0.321	0.196	0.130	0.085
Cd	0.060	0.095	0.072	0.041	0.063	0.043	0.041	0.051	0.057	0.044	0.058	0.052
Sb	0.460	0.718	0.686	0.485	0.679	0.532	0.570	0.648	0.699	0.727	0.501	0.565
Cs	4.97	2.99	3.17	2.38	3.20	2.70	2.83	3.15	3.16	3.28	2.67	2.73
Ba	533	454	497	629	530	469	517	503	447	435	458	462
Tl	0.462	0.439	0.374	0.443	0.480	0.387	0.398	0.386	0.387	0.420	0.397	0.408
Pb	14.6	13.6	13.8	14.0	15.0	13.0	13.5	14.4	14.1	13.4	12.7	13.1
Bi	0.105	0.116	0.335	0.099	0.131	0.104	0.091	0.152	0.136	0.125	0.089	0.103
Th	5.22	5.33	5.81	5.32	4.90	4.41	3.84	5.09	5.45	4.67	3.68	4.03
U	1.60	1.15	1.36	1.10	1.09	0.879	0.871	1.14	1.20	1.02	0.855	0.830

Table 1 (*continued*)

Samples	ML14	K1	K2	K3	K4	K5	K6	K7	K8	K9	K10	K11
Nb	7.37	7.41	8.46	7.10	7.55	5.22	5.68	6.89	7.49	5.94	4.17	4.85
Ta	0.491	0.624	0.619	0.543	0.879	0.442	0.410	0.529	0.624	0.481	0.324	0.382
Zr	170	216	278	269	182	147	135	167	214	147	93.3	109
Hf	4.50	5.77	7.26	6.53	4.67	3.73	3.56	4.56	5.76	3.88	2.64	2.92
La	23.0	16.6	21.0	18.6	16.2	13.1	13.1	16.1	18.0	15.6	11.3	12.7
Ce	41.2	31.6	38.3	33.4	30.2	24.0	23.6	29.9	33.2	28.1	20.5	23.0
Pr	4.92	3.71	4.59	3.97	3.53	2.82	2.77	3.42	3.92	3.30	2.39	2.71
Nd	18.9	14.3	17.7	15.3	13.8	10.9	10.7	13.2	15.1	12.6	9.29	10.5
Sm	3.34	2.71	3.28	2.74	2.55	2.02	1.98	2.46	2.78	2.31	1.75	1.98
Eu	0.767	0.588	0.738	0.593	0.553	0.461	0.510	0.563	0.613	0.554	0.479	0.441
Gd	2.77	2.24	2.79	2.30	2.27	1.77	1.69	1.93	2.36	1.98	1.52	1.62
Tb	0.468	0.411	0.516	0.419	0.380	0.276	0.307	0.378	0.403	0.357	0.258	0.312
Dy	2.53	2.20	2.90	2.13	2.06	1.74	1.81	2.10	2.12	2.03	1.54	1.69
Ho	0.480	0.425	0.504	0.418	0.401	0.328	0.321	0.425	0.443	0.364	0.307	0.331
Er	1.41	1.29	1.61	1.35	1.25	1.02	1.02	1.22	1.29	1.11	0.951	0.901
Tm	0.268	0.222	0.266	0.215	0.213	0.150	0.186	0.221	0.229	0.201	0.163	0.165
Yb	1.62	1.38	1.61	1.47	1.33	1.02	0.995	1.20	1.48	1.25	0.940	0.992
Lu	0.219	0.185	0.247	0.217	0.207	0.162	0.146	0.201	0.212	0.177	0.150	0.142
Eu/Eu*	0.78	0.73	0.75	0.73	0.71	0.75	0.86	0.79	0.74	0.80	0.90	0.76
Th/U	3.26	4.63	4.27	4.84	4.50	5.02	4.41	4.46	4.54	4.58	4.30	4.86
ΣREE	101.9	77.9	96.1	83.1	74.9	59.8	59.1	73.3	82.2	69.9	51.5	57.5

Samples	K12	K13	K14	KF1	KF2	KF3	KF4	KF5	KF6	KF7	KF8	KF9
SiO_2	77.12	77.22	78.77	74.02	73.38	70.31	70.35	71.93	73.01	73.41	73.71	67.09
Al_2O_3	9.06	8.63	8.25	9.84	9.45	9.88	9.82	9.51	9.61	9.86	9.97	9.81
Fe_2O_3	2.34	2.63	2.10	3.15	2.65	3.97	4.07	3.13	2.85	3.12	3.30	5.19
CaO	2.62	2.93	2.76	3.24	4.30	4.77	4.81	4.61	4.43	3.20	3.40	5.67
MgO	0.93	0.96	0.92	1.17	1.15	1.34	1.27	1.21	1.12	1.16	1.27	1.50
K_2O	1.96	1.76	1.85	1.88	1.93	1.88	1.82	1.84	1.90	1.93	1.97	1.79
Na_2O	1.99	1.83	1.79	2.09	2.07	2.07	2.05	2.01	2.08	2.08	2.09	1.90
TiO_2	0.38	0.38	0.30	0.58	0.47	0.80	0.78	0.54	0.47	0.53	0.58	0.87
MnO	0.04	0.05	0.04	0.06	0.05	0.08	0.09	0.06	0.06	0.06	0.06	0.10
LOI	2.53	2.93	3.06	2.90	4.08	3.89	4.41	4.73	4.68	3.56	3.99	5.36
CIA	51.09	52.11	51.09	52.46	51.48	52.75	52.97	52.48	51.90	52.45	52.52	54.49
Li	18.5	16.9	18.4	22.0	19.0	18.9	21.9	20.7	21.4	21.7	20.9	23.2
Be	0.850	1.37	0.952	1.27	1.22	0.943	1.71	0.934	1.37	1.36	1.52	1.20
Sc	6.35	6.66	5.22	8.71	7.24	9.23	10.1	8.31	7.36	7.98	8.10	11.3
V	39.4	48.2	39.4	59.9	48.5	76.9	74.4	57.3	51.2	58.2	58.6	101
Cr	43.8	54.6	36.3	87.2	44.5	91.5	97.6	70.3	57.8	60.7	65.6	178
Co	5.72	6.50	5.17	7.91	6.71	8.73	9.75	7.70	7.47	7.55	7.24	11.0
Ni	13.1	13.0	11.7	22.2	15.9	20.4	21.1	18.9	17.9	18.3	17.6	24.4
Cu	8.63	9.08	8.94	13.8	13.5	18.9	19.3	13.9	14.2	13.0	14.0	17.4
Zn	30.3	28.8	27.7	43.5	36.2	45.5	48.2	39.8	38.4	41.3	42.4	54.9
Ga	9.42	9.01	8.66	11.0	10.4	11.5	11.8	10.4	10.5	10.6	10.8	12.4
Rb	73.1	67.0	68.7	70.9	67.9	66.8	69.2	68.8	71.0	71.7	68.6	70.0
Sr	188	188	174	192	206	207	222	209	208	189	177	221
Y	12.9	14.1	11.8	17.2	16.4	20.3	22.9	17.7	16.3	16.7	17.5	25.6
Mo	0.181	0.253	0.204	1.10	0.285	0.448	0.471	0.366	0.386	0.382	0.409	0.540
Cd	0.068	0.059	0.037	0.148	0.060	0.061	0.151	0.128	0.057	0.060	0.048	0.134
Sb	0.655	0.763	0.683	0.841	0.828	0.935	0.991	0.996	0.910	0.795	0.881	1.35
Cs	3.32	3.28	3.20	3.65	3.26	3.30	3.64	3.60	3.63	3.67	3.50	3.96
Ba	481	428	449	449	448	432	457	434	457	449	396	404
Tl	0.427	0.434	0.448	0.433	0.368	0.391	0.419	0.400	0.375	0.371	0.378	0.386
Pb	14.1	13.9	13.9	15.2	13.0	14.7	16.9	14.8	15.3	15.3	15.5	18.8
Bi	0.126	0.155	0.151	0.197	0.151	0.224	0.261	0.187	0.196	0.179	0.198	0.304
Th	5.29	5.27	5.05	6.83	6.60	9.40	9.23	7.12	6.48	7.53	8.41	11.2
U	1.26	1.19	1.17	1.47	1.43	1.84	1.80	1.43	1.32	1.47	1.69	2.20
Nb	7.94	8.28	6.24	12.0	9.55	14.6	16.6	11.3	10.4	11.1	11.4	17.8
Ta	0.625	0.638	0.539	0.862	0.744	1.15	1.27	0.881	1.03	0.844	0.945	1.52
Zr	246	195	157	155	149	245	213	161	116	135	181	235
Hf	6.87	5.22	4.22	4.16	3.97	6.63	5.57	4.49	3.25	3.42	4.78	5.82
La	17.2	16.9	15.7	23.2	23.7	30.9	31.0	23.5	22.4	24.3	26.5	35.5
Ce	32.0	31.0	29.1	44.4	43.3	58.2	59.4	44.0	42.4	46.0	50.4	67.3
Pr	3.78	3.70	3.41	5.26	5.26	7.09	7.18	5.28	5.12	5.41	5.94	8.23
Nd	14.7	14.4	13.1	20.4	20.4	27.3	27.5	20.0	19.8	20.4	22.9	31.2
Sm	2.71	2.72	2.52	3.79	3.74	4.76	5.08	3.70	3.75	3.76	4.23	5.89
Eu	0.672	0.642	0.591	0.742	0.762	0.932	0.918	0.730	0.704	0.789	0.842	0.995
Gd	2.36	2.51	2.10	3.27	3.01	4.12	3.97	3.34	2.80	3.08	3.45	4.86
Tb	0.412	0.429	0.393	0.625	0.524	0.740	0.735	0.544	0.537	0.586	0.629	0.967
Dy	2.40	2.49	2.01	2.93	2.90	3.71	3.67	2.82	2.73	2.90	3.04	4.37
Ho	0.463	0.501	0.403	0.587	0.583	0.736	0.734	0.633	0.595	0.591	0.673	0.912
Er	1.40	1.47	1.22	1.80	1.58	2.07	2.22	1.69	1.47	1.67	1.83	2.52
Tm	0.265	0.227	0.195	0.317	0.318	0.352	0.365	0.302	0.306	0.294	0.337	0.445
Yb	1.60	1.53	1.13	1.94	1.76	2.34	2.34	1.83	1.70	1.80	2.13	2.67
Lu	0.203	0.224	0.179	0.262	0.216	0.321	0.305	0.233	0.208	0.233	0.254	0.350

(*continued on next page*)

Table 1 (*continued*)

Samples	K12	K13	K14	KF1	KF2	KF3	KF4	KF5	KF6	KF7	KF8	KF9
Eu/Eu*	0.82	0.76	0.79	0.65	0.70	0.65	0.63	0.64	0.67	0.71	0.68	0.57
Th/U	4.20	4.43	4.32	4.65	4.62	5.11	5.13	4.98	4.91	5.12	4.98	5.09
ΣREE	80.2	78.7	72.1	109.5	108.1	143.6	145.4	108.6	104.5	111.8	123.2	166.2

Samples	KF10	KF11	KF12	KF13	KF14	KS1	KS2
SiO_2	69.26	67.05	71.58	61.03	69.76	59.87	43.26
Al_2O_3	10.14	9.93	9.78	9.63	9.73	14.02	10.15
Fe_2O_3	4.68	5.73	3.67	8.11	4.10	3.65	4.75
CaO	5.09	5.54	4.25	7.16	5.33	4.71	18.27
MgO	1.53	1.49	1.37	1.81	1.58	2.79	1.67
K_2O	1.84	1.77	1.83	1.65	1.87	2.80	2.16
Na_2O	1.99	1.93	2.00	1.69	1.91	1.40	1.53
TiO_2	0.82	1.02	0.71	1.35	0.69	0.81	0.43
MnO	0.10	0.11	0.07	0.15	0.08	0.06	0.08
LOI	4.89	4.89	4.16	6.47	5.25	9.69	17.83
CIA	54.27	54.56	53.31	56.71	53.92	64.71	57.91
Li	22.7	25.9	21.0	23.1	21.6	19.4	21.4
Be	1.23	1.55	0.92	1.12	1.32	1.15	1.39
Sc	10.5	11.9	9.40	15.0	10.0	11.0	8.52
V	83.2	112	69.4	161	74.7	87.7	62.7
Cr	135	220	104	333	122	145	138
Co	10.1	11.8	8.35	14.2	8.95	14.0	10.3
Ni	23.4	26.9	20.3	30.9	22.3	21.1	21.0
Cu	15.6	17.8	13.5	22.0	19.9	12.1	10.0
Zn	49.9	60.3	47.2	71.6	49.9	57.1	41.7
Ga	11.9	13.6	11.5	14.0	11.7	16.6	12.8
Rb	67.0	70.9	68.8	65.2	68.9	80.5	65.5
Sr	202	221	201	236	212	511	391
Y	22.4	31.1	20.9	33.4	21.0	18.8	22.3
Mo	0.537	0.596	0.579	0.782	0.495	1.02	1.13
Cd	0.147	0.105	0.101	0.078	0.129	0.059	0.160
Sb	1.13	1.30	0.983	2.00	1.04	0.082	0.137
Cs	3.62	3.89	3.69	3.83	3.71	2.94	3.49
Ba	391	422	419	351	397	746	642
Tl	0.380	0.379	0.405	0.398	0.339	0.484	0.34
Pb	16.7	18.7	13.8	22.8	15.8	9.53	12.4
Bi	0.262	0.286	0.204	0.491	0.243	0.070	0.079
Th	7.54	12.8	8.93	16.1	8.94	4.55	6.61
U	1.82	2.51	1.84	3.26	1.83	0.993	0.959
Nb	16.6	20.4	14.5	26.4	13.5	10.8	7.69
Ta	1.50	1.48	1.18	2.11	1.17	0.605	0.474
Zr	196	361	242	382	168	374	251
Hf	4.99	9.11	6.08	9.57	4.71	9.52	6.33
La	26.4	37.5	31.6	48.7	29.8	32.7	33.2
Ce	50.2	71.2	60.2	93.0	55.6	64.1	59.5
Pr	6.09	8.51	7.08	11.3	6.69	7.97	7.23
Nd	23.2	32.3	26.8	43.1	25.5	32.5	28.7
Sm	4.41	6.09	4.94	8.05	4.62	5.85	5.16
Eu	0.928	1.21	0.882	1.29	0.916	1.37	1.19
Gd	4.08	5.47	3.71	6.78	4.05	4.63	4.49
Tb	0.741	1.06	0.723	1.32	0.759	0.707	0.750
Dy	3.90	5.32	3.59	6.02	3.60	3.61	3.81
Ho	0.766	1.16	0.714	1.25	0.735	0.622	0.711
Er	2.16	2.98	1.95	3.36	1.97	1.85	2.07
Tm	0.363	0.496	0.325	0.602	0.372	0.284	0.348
Yb	2.58	3.47	2.21	3.79	2.23	1.79	1.92
Lu	0.332	0.459	0.305	0.427	0.280	0.259	0.279
Eu/Eu*	0.67	0.64	0.63	0.54	0.65	0.81	0.76
Th/U	4.14	5.10	4.85	4.94	4.89	4.58	6.89
ΣREE	126.2	177.2	145.0	229.0	137.1	158.2	149.4

patterns of bulk and fine aeolian sand samples from the Kubuqi Desert are quite consistent, but with obviously higher Sb and Cr concentrations than those in sandstone samples of the region (Fig. 4).

Ratios of trace elements may provide references for estimation of source areas. The element La and Th show a good linear relationship for many sediments and rocks, with La/Th ratios varying between 1 and 10 (Fig. 5a). Aeolian sand in the western Maowusu Sandy Land and the Kubuqi Desert have an average La/Th ratio of 3.2, slightly higher than the UCC (McLennan, 2001). Sandstones and lacustrine sediment samples have La/Th ratios fluctuating around 5, similar to those of aeolian sand samples in the eastern Maowusu Sandy Land. Plots of Th/Co vs. La/Sc diagram have been used to differentiate between silicic and basic sources (Cullers, 2002). Co and Sc are enriched in basic rocks, whereas Th and La are enriched in felsic rocks. In addition, La-Th-Sc ternary plots are effective in provenance analysis (Taylor and McLennan, 1985; Cullers, 2002). All samples in our study fall into the areas of silicic rocks in both diagrams (Fig. 5b, c), thus suggesting a silicic origin. Cr and Ni are enriched in mafic rocks, whereas Y and V are enriched in felsic rocks. Thus, on a Y/Ni vs. Cr/V diagram, mafic-ultramafic rocks such as ophiolite plot with lower Y/Ni and higher Cr/V, while felsic rocks such as granite plot with higher Y/Ni and lower Cr/V (Amorosi et al., 2002). Samples collected in the Maowusu and Kubuqi occupy different fields in the Y/Ni vs. Cr/V diagram (Fig. 5d). Lacustrine sediments and sandstones show a wide variation. Some samples have lower Y/Ni and higher

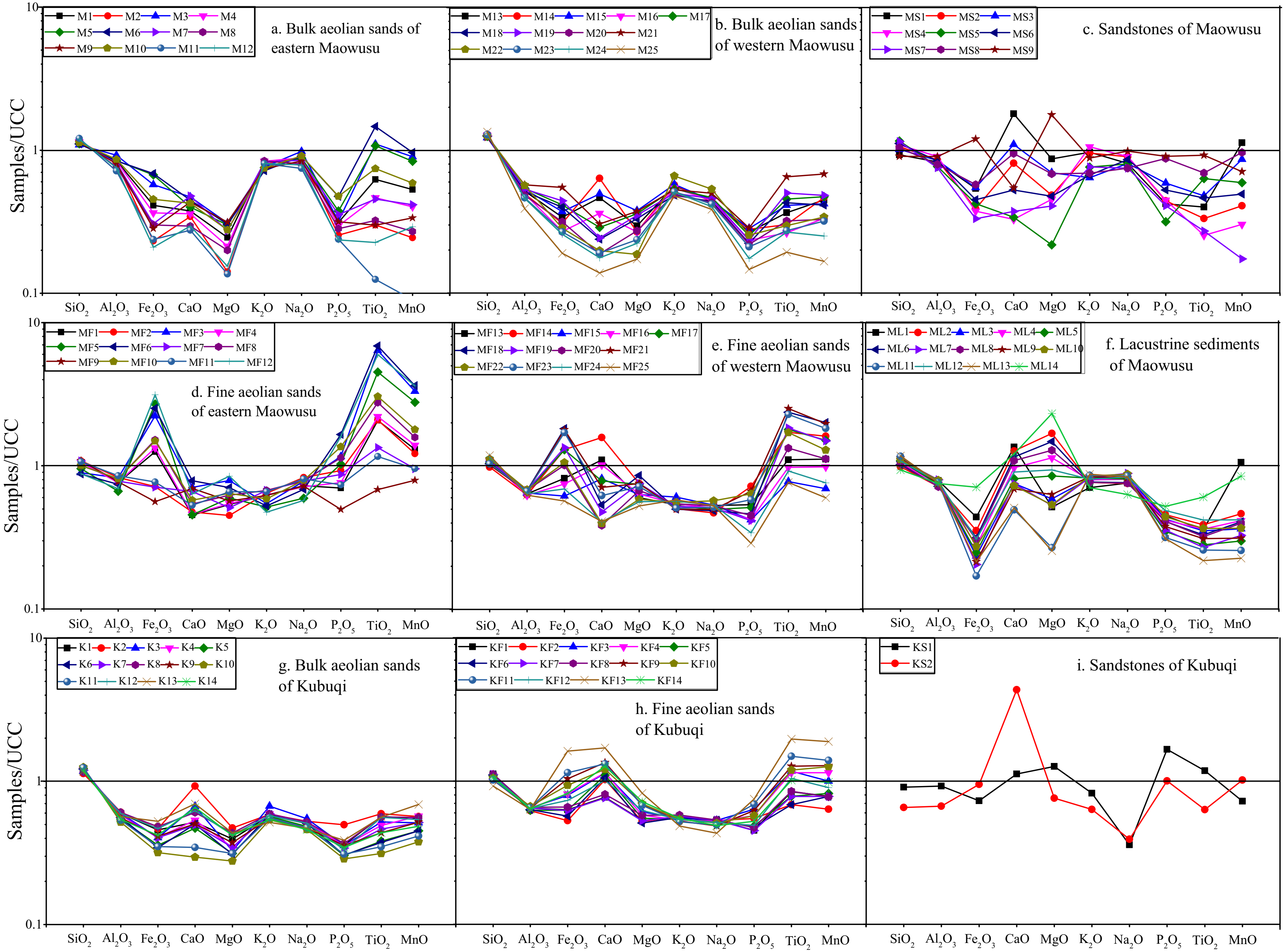

Fig. 3. UCC-normalized diagrams of major elements. UCC values from McLennan (2001).

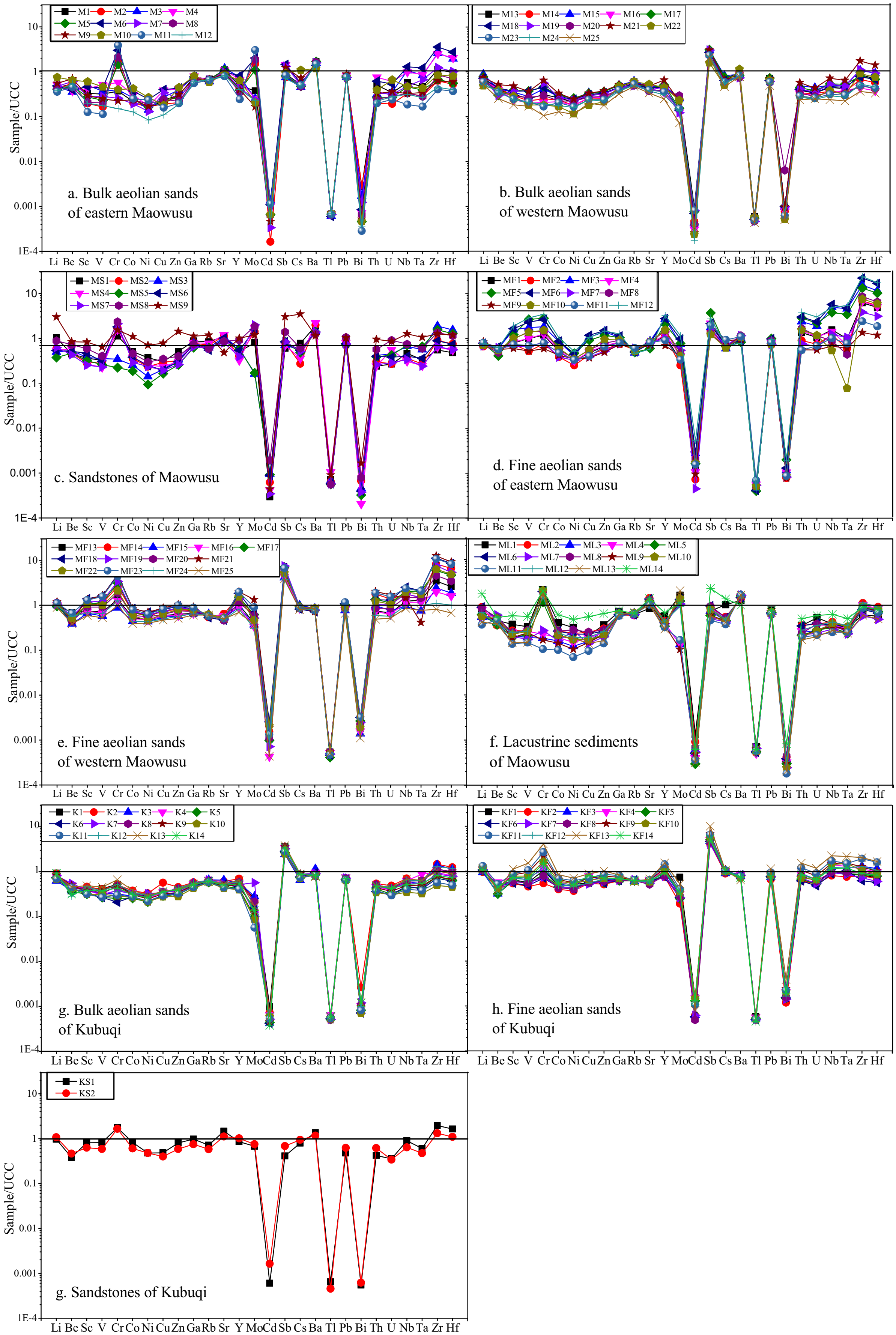

Fig. 4. UCC-normalized distribution patterns of trace elements for all samples in the Ordos Deserts. UCC values from McLennan (2001).

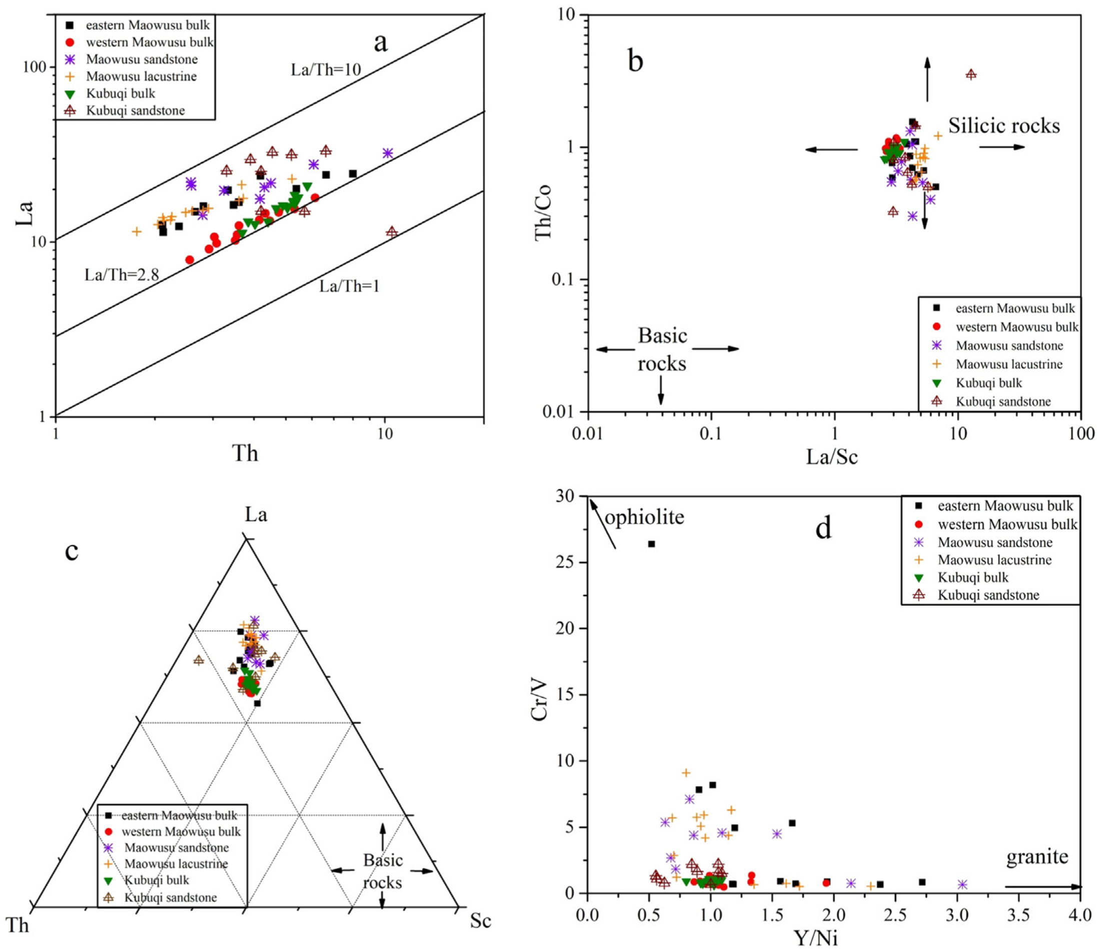

Fig. 5. La-Th diagram (a), plot of Th/Co vs. La/Sc (b), La-Th-Sc ternary diagram (c) and plot of Cr/V vs. Y/Ni (d) for samples in the Ordos Deserts. Supplementary data for sandstones in the Kubuqi Desert from Rao et al. (2011a).

Cr/V, others have higher Y/Ni and lower Cr/V. Aeolian sands in the eastern Maowusu plot in similar areas with sandstones and lacustrine sediment, while aeolian sands in the western Maowusu and Kubuqi show quite consistent Y/Ni and Cr/V ratios. Most samples fall close to the granite end member, with the amount of ultra-mafic fraction < 5% (Amorosi et al., 2002). Therefore, aeolian sands in the Ordos Deserts have a silicic crustal origin.

4.3. Rare earth elements (REE)

Of all the samples collected in the Maowusu Sandy Land, the mean total REE contents are quite different between the eastern and the western provinces, i.e., 78.6 ppm in bulk sand samples from the eastern province and 56.4 in bulk sand samples from the western province. The mean total REE concentrations are 96.6 ppm in the sandstone samples and 72.1 ppm in lacustrine sediments of the Maowusu. The fine fractions have significantly higher REE concentrations than bulk sand samples, with an average of 275.5 ppm in eastern and 177.5 ppm in western area. The samples of Kubuqi Desert show a mean total REE of 72.6 ppm in bulk sand samples, 138.2 ppm in fine fractions and 153.8 ppm in sandstone samples (Table 1).

The chondrite-normalized distribution patterns of all samples show steep light-REE and flat heavy-REE, identical with that of UCC (Fig. 6). Sand samples of the western Maowusu Sandy Land and the Kubuqi Desert have negative Eu anomalies, with Eu/Eu* values from 0.71 to 0.90. Eu anomalies are more negative (i.e. lower) in the fine fractions, with average Eu/Eu* values of 0.56 in the eastern Maowusu, 0.57 in the western Maowusu and 0.64 in the Kubuqi Desert. Large variations of Eu anomalies occur in lacustrine and sandstone samples of the Maowusu, and also in the sand samples of the eastern province (Table 1). About half of these samples have slightly negative Eu anomalies, while other samples have no obvious or even positive Eu anomalies (Table 1 and Fig. 6). Lower Eu anomalies in aeolian sand samples of the western Maowusu may suggest a depletion of feldspar. This is consistent with the major element compositions (Fig. 3), indicating that the aeolian sand samples in the western Maowusu have lower contents of Al_2O_3, K_2O and Na_2O.

The Eu/Eu* values are anti-correlated with the total REE in the same kinds of samples, especially between fine fractions and their bulk aeolian samples, i.e., the higher the total REE, the lower the Eu/Eu* value (Fig. 7).

5. Discussion

5.1. Provenances of aeolian sands in the eastern Maowusu Sandy Land

Mineralogical maturity is defined as a compositional state of a clastic sediment body with regard to its concentrations of resistant minerals, mainly quartz (Blatt et al., 1972; Pettijohn et al., 1972), which can provide new insights in the origin and evolution of sediments (Muhs, 2004; Muhs et al., 2013). Mineralogical maturity can be illustrated by a diagram of $\log(Na_2O/K_2O)$ vs. $\log(SiO_2/Al_2O_3)$, where the Na_2O/K_2O is a measure of the plagioclase to K-feldspar ratio while SiO_2/Al_2O_3 is a measure of quartz to total feldspar (Pettijohn et al., 1972). Sediments with higher degree of mineralogical maturity have higher $\log(SiO_2/Al_2O_3)$ and lower $\log(Na_2O/K_2O)$ (Muhs et al., 2013).

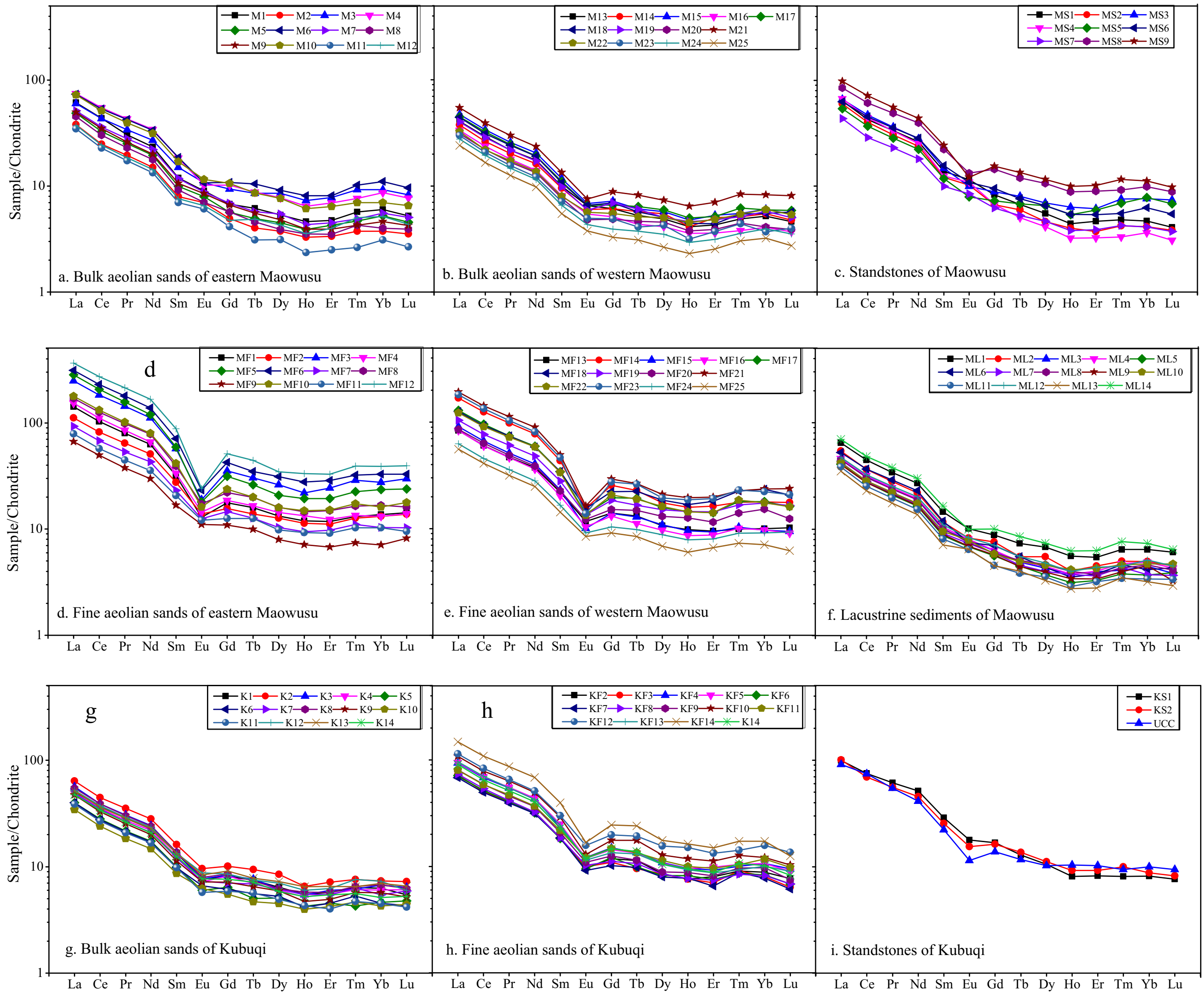

Fig. 6. Chondrite-normalized REE patterns for all samples in the Ordos Deserts. UCC values from McLennan (2001).

Aeolian sands of the western Maowusu Sandy Land show significantly higher $\log(SiO_2/Al_2O_3)$ compared with those of the eastern province, indicating that they contain more quartz and less feldspar. Fine fractions are mineralogically immature relative to bulk sand samples. Aeolian sands of the eastern Maowusu Sandy Land have a similar compositional range as the sandstones and lacustrine sediments nearby.

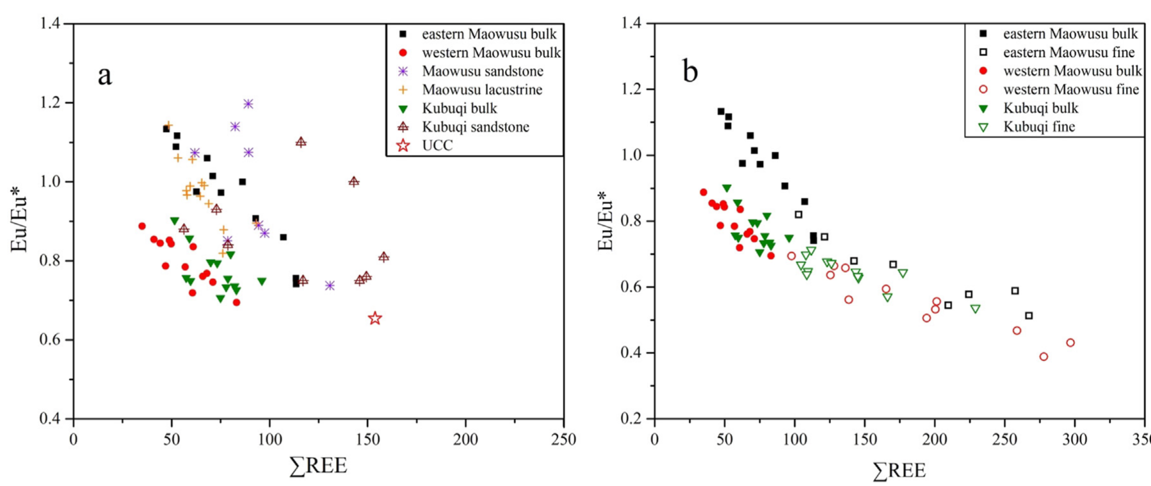

Fig. 7. Diagrams of Eu/Eu* vs. ∑REE for all samples in the Ordos Deserts. UCC values from McLennan (2001). Supplementary data for sandstones in the Kubuqi Desert from Rao et al. (2011a).

Notably, both the bulk aeolian sand samples and their fine fractions of the Kubuqi Desert have a similar degree of mineralogical maturity as those of the western Maowusu (Fig. 8).

Several factors may explain the different degree of mineralogical maturity of aeolian sands in the eastern and western Maowusu Sandy Land. Certainly, sources have a great influence in this regard (Pettijohn et al., 1972; Muhs, 2004; Muhs et al., 2013). Desert sands with high degree of mineralogical maturity may simply inherit their composition from quartz-rich sedimentary bodies or rocks (Muhs, 2004). Chemical and physical weathering during the production, transportation and deposition can also result in reduction of feldspar and lithic particle abundance, and hence cause greater mineralogical maturity (Dutta et al., 1993; Nesbitt et al., 1996, 1997). However, the processes of chemical weathering are very slow and need a long time even in favorable climatic conditions. The average CIA values of aeolian sands are 52.5 in the eastern Maowusu and 53.1 in the western Maowusu, suggesting minimal chemical weathering. Although it is more humid in the eastern Maowusu Sandy region, it seems that chemical weathering is not the main cause for the difference between eastern and western province because the average CIA is higher in the drier region.

Physical weathering and associated deflation are likely to have an influence on the composition and mineralogy of aeolian sands in arid and semi-arid areas (Muhs, 2004). Laboratory experiments show that K-feldspar may break into silt sizes during ballistic impacts under strong winds (>10 ms^{-1}) (Dutta et al., 1993), and silt-sized K-feldspar grains are then removed from a dune field by deflation, leaving a sand-sized quartz-rich residue. Crouvi et al. (2012) reported that aeolian abrasion should be the primary mechanism in dust production of sand deserts. However, the effect of aeolian abrasion during transport may have been overestimated (Garzanti et al., 2012; Garzanti et al., 2015), and mechanical processes can be held responsible for only minor compositional changes even after aeolian transport over distances of many hundred kilometers (Garzanti et al., 2012).

Abrasion and impacts during fluvial transport may also have influences (Pittman, 1969; Cameron and Blatt, 1971), because these processes will result in size reduction of feldspar and other minerals with low hardness. Silt-sized particles of feldspar remain in suspension and then are carried downstream, improving mineralogical maturity of detrital sand-sized fluvial sediments (Muhs, 2004). But a great number of studies have shown little change in the amount of quartz relative to feldspar or lithic fragments as a function of distance downstream in most rivers (Hayes, 1962; Nesbitt and Young, 1996), and the supply of local sediments is generally regarded to be responsible for downstream changes in the relative abundances of different minerals (Hayes, 1962). Most rivers in the Maowusu are seasonal and have limited runoff, hence they should have little influence on mineralogical maturity. Thus, different provenance rather selective chemical and physical weathering and deflation is inferred to be the most important factor that results in different degree of mineralogical maturity between aeolian sands in the eastern and western Maowusu.

Different Eu anomalies and REE contents also occur between the aeolian sand samples of the eastern and western Maowusu Sandy Land (Figs. 6, 7). Two possible mechanisms may cause such distinct variation of Eu anomalies in aeolian sediments via mineralogical differentiation, i.e., wind sorting and different provenance. Wind sorting may result in enrichment of heavy minerals and depletion in feldspar, quartz and lithic fragments (Garzanti et al., 2012), and thus produces aeolian sands with high total REE contents and low Eu/Eu* values. However, as shown in Fig. 7a, aeolian sand samples in the western Maowusu have similar total REE contents but clearly lower Eu/Eu* values compared with those in the eastern Maowusu, excluding obvious wind impact on mineralogical differentiation. Thus, we consider different provenance also as the most likely reason for the differences in Eu anomalies between the aeolian sand samples of the eastern and western Maowusu.

Aeolian sands in the eastern Maowusu Sandy Land have a similar degree of mineralogical maturity, Eu anomalies, and La/Th values in comparison with sandstones and lacustrine sediments, suggesting a genetic link between them. Sandstones of different geological periods and lacustrine sediments of dry lakes are widely distributed in the Maowusu and southern Kubuqi (Zhu et al., 1980; Rao et al., 2011a, 2011b). Their weak cementation makes them easily weathered and produces large quantities of sand-sized particles, that may provide plentiful detrital materials for aeolian entrainment (Zhu et al., 1980; Rao et al., 2011a, 2011b; Stevens et al., 2013). As shown in Fig. 9, most aeolian sands of the eastern Maowusu are placed in the same field as sandstones and lacustrine sediments, reconfirming that underlying sandstones and local lacustrine sediments are their main sources. However, aeolian sands in the western Maowusu and Kubuqi have similar degrees of mineralogical maturity and REE compositions, and only a small number of them fall into the field of sandstones and lacustrine sediments (Figs. 7, 8, 9), supporting the interpretation that the aeolian sands in the western Maowusu and Kubuqi may have the same external sources but the underlying sandstones and lacustrine sediments are not their primary sources.

In general, fine fractions of aeolian sands have higher total REE, lower Eu/Eu* and mineralogical maturity than their bulk samples (Figs. 7, 8). However, fine fractions have trace element compositions similar to bulk aeolian sand samples, except for their Eu/Eu* values (Fig. 10). It is likely that mineralogical differentiation during wind-sorting rather than difference in provenance causes the difference in

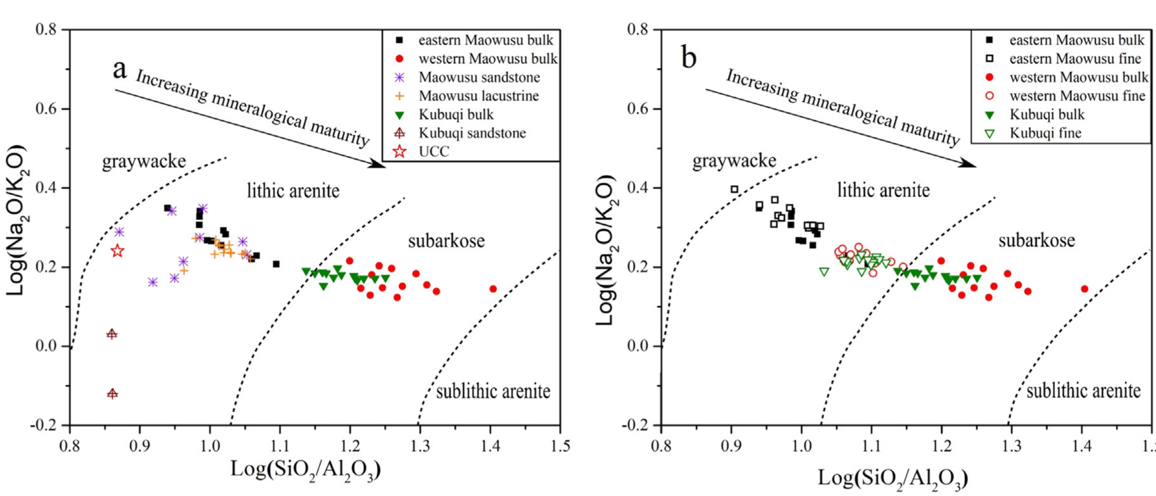

Fig. 8. Plots of Log(Na_2O/K_2O) vs. Log(SiO_2/Al_2O_3) for sediments in the Ordos Deserts. UCC (Taylor and McLennan, 1985; McLennan, 2001).

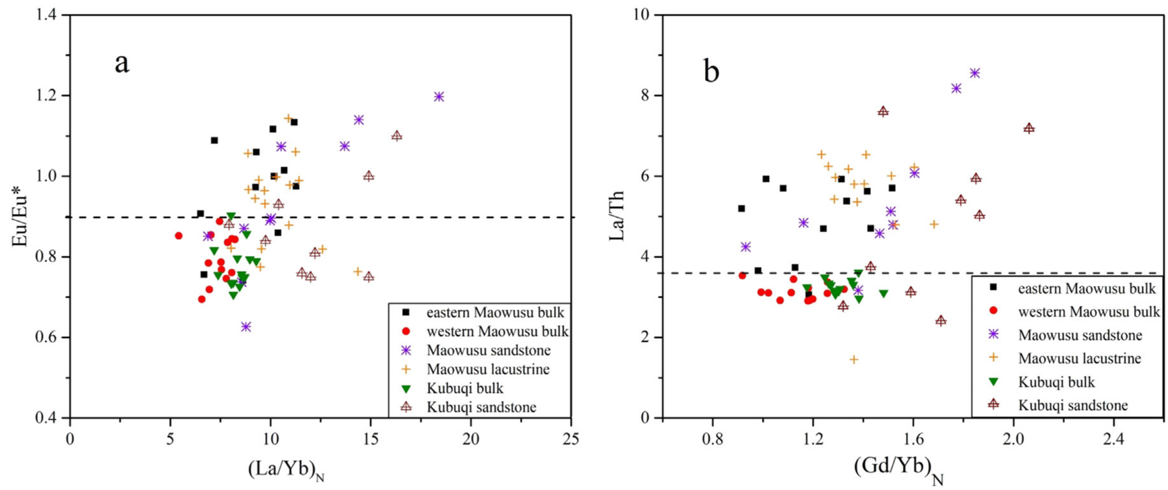

Fig. 9. Plots of Eu/Eu* vs. $(La/Yb)_N$ (a) and La/Th vs. $(Gd/Yb)_N$ (b) for sediments in the Ordos Deserts. Supplementary data for sandstones in the Kubuqi Desert from Rao et al. (2011a).

Eu/Eu* values and mineralogical maturity between the fine and bulk aeolian sand samples. As the case in other deserts demonstrates, the fine fractions of aeolian sands are often made up of sediments from various origins due to mixing during aeolian transportation, also causing differences in geochemical characteristics between the fine fractions and their contiguous bulk samples (Yang et al., 2007b).

5.2. Provenance of aeolian sands in the western Maowusu Sandy Land and the Kubuqi Desert

Grain size data for aeolian sands in the western Maowusu Sandy Land and the Kubuqi Desert show that most aeolian sand samples contain <5% silt and clay (Shu et al., 2016; Yang et al., 2016), and particles coarser than silt are transported for much shorter distances than silts (Zhu et al., 1981; Yang et al., 2007b). Previous provenance studies suggested that detritus produced by tectonic activities, glacial grinding, frost weathering, salt weathering, and fluvial comminution are important sources of Quaternary aeolian deposits (Yang, 1991; Goudie, 2002; Stevens et al., 2013), and rivers play significant roles in transporting debris from source areas to deposition areas (Liu and Yang, 2013; Stevens et al., 2013; Lancaster et al., 2015; Hu and Yang, 2016; Yang and Eitel, 2016). The Helan Mountains and the Yinshan Mountains lie in the upwind direction of the Ordos Deserts on the other side of the Yellow River (Figs. 1, 2), and their mountainous processes may produce mass detritus for the desert sands. However, significant differences in trace element compositions rule out sediments from the Helan Mountains and the Yinshan Mountains as sources of sands in the western Maowusu Sandy Land and the Kubuqi Desert (Fig. 11a, b). Felsic rocks of the Helan Mountain have much higher $(La/Yb)_N$, $(Gd/Yb)_N$ and slightly lower La/Th values, while felsic rocks of the Yinshan Mountain have higher $(La/Yb)_N$, $(Gd/Yb)_N$ and La/Th values. The Yellow River, characterized by abundant fluvial deposits, also lies upwind of the Ordos Deserts (Fig. 2). Its fluvial sediments have similar trace element characteristics to the aeolian sands in the western Maowusu and Kubuqi (Fig. 11c, d), suggesting that fluvial sediments of the Yellow River are likely the primary sources for the western Maowusu Sandy Land and the Kubuqi Desert, and the rocks providing sediments for the Yellow River are their original sources.

In light of geological and geographical features, the Yellow River can be divided into the upper, the middle and the lower reaches (Ran et al., 2009). The upper section of the Yellow River can be subdivided into two different parts. The section above Qingtong Gorge is characterized by erosional processes and the river course below Qingtong Gorge is characterized by fluvial deposition (Ran et al., 2009) (Fig. 1). Because of the high topographic gradient in the upper section, the river flows rapidly and produces deep canyons and transports large amounts of sediment downstream (Ran et al., 2009; Su, 2013). Downstream of Qingtong Gorge, the Yellow River leaves the northeastern Tibetan Plateau. The

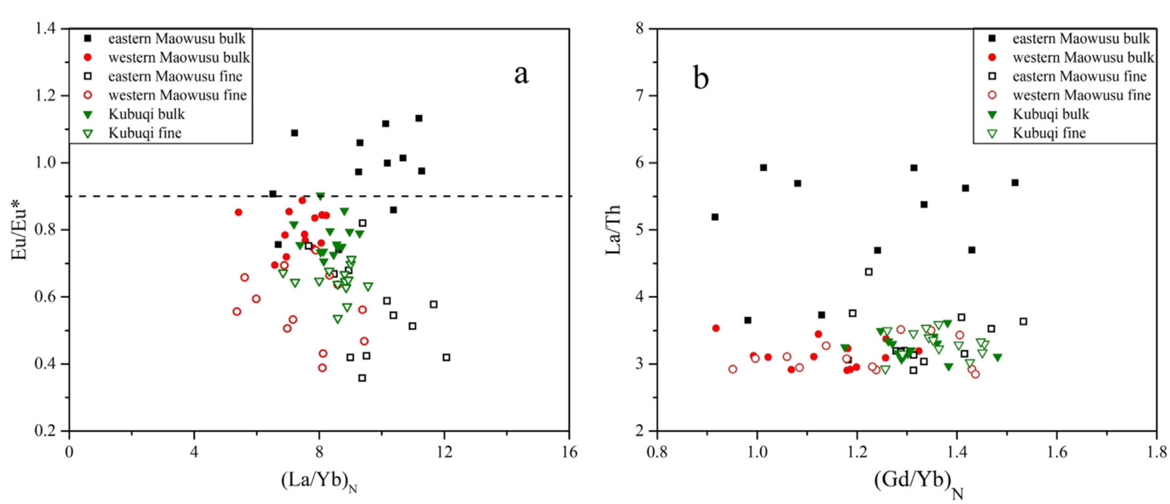

Fig. 10. Plots of Eu/Eu* vs. $(La/Yb)_N$ (a), La/Th vs. $(Gd/Yb)_N$ (b) for fine fractions and their bulk aeolian samples in the Ordos Deserts.

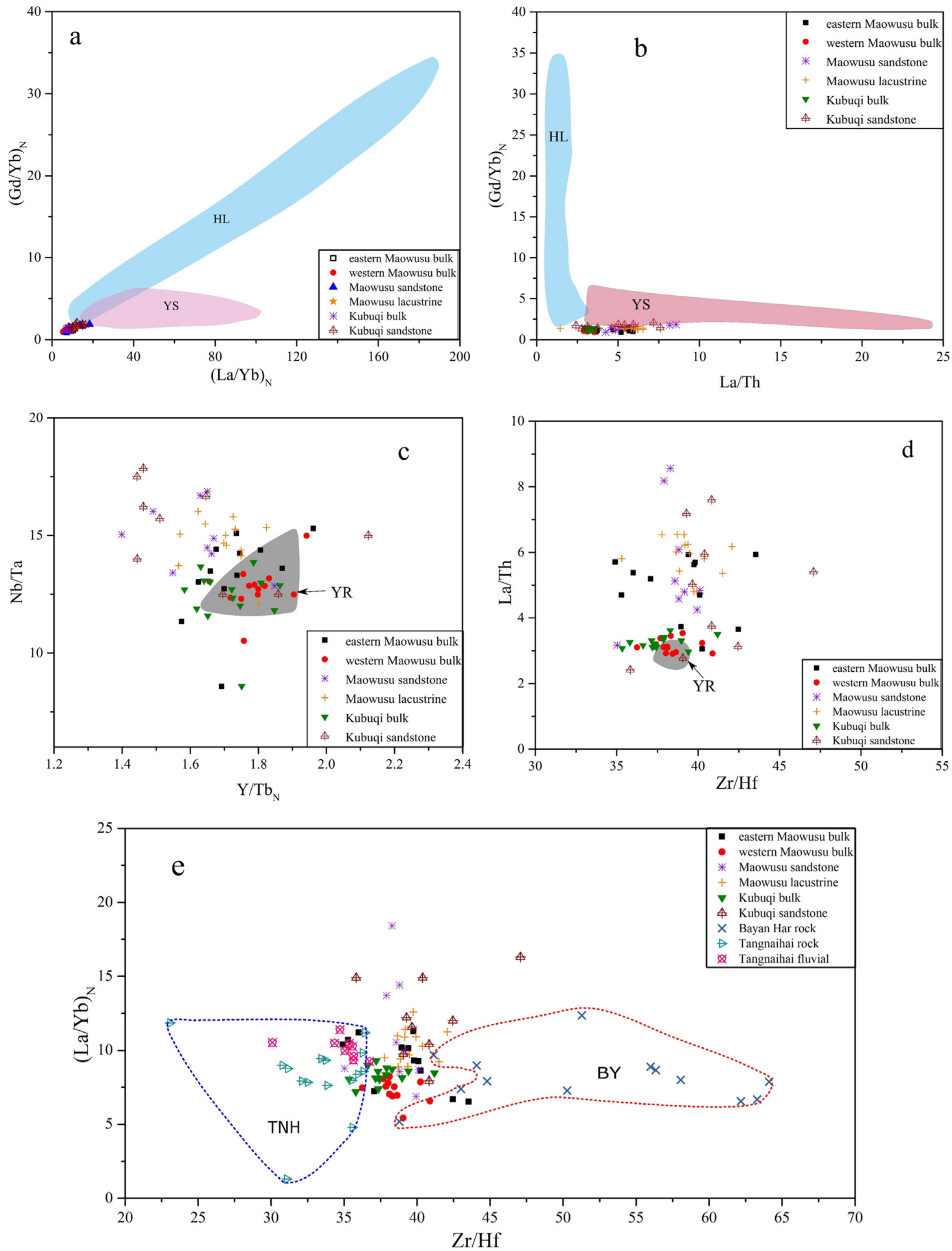

Fig. 11. Bivariate diagrams of trace and rare earth element ratios of samples from the Ordos Deserts and the sediments of the Ningxia-Inner Mongolian section along the Yellow River, compared with their potential source areas. HL refers to the data from rocks in the Helan Mountains (Li et al., 2013; Liu et al., 2016); YS marks the data from rocks in the Yinshan Mountains (Yan et al., 2001; Lin, 2011).YR—Fluvial sediments in the Ningxia-Inner Mongolian section of the Yellow River (data from Rao et al., 2011a); BY—Felsic rocks on the north side of the Bayan Har Mountains (Fig. 1) (data from She et al., 2006); TNH—Rocks around the Tangnaihai hydrological station (Fig. 1) (data from Fang, 2010).

reduced fluvial gradient downstream of the Tibetan Plateau results in considerable sediment deposition (Shi et al., 2013; Su, 2013), especially sand-sized particles (Ran et al., 2009). This provides abundant potential material for aeolian reworking and transportation, aided by the arid and semi-arid climate in this region. Thus, it is reasonable to deduce that detrital materials brought from the NE Tibetan Plateau by the Yellow River, deposited in the Ningxia-Inner Mongolian section, are the primary provenance of the aeolian sands in the western Maowusu and Kubuqi, thus supporting our interpretation of trace element data. The similar zircon age profiles of the sediments in the western Maowusu, the Loess Plateau and the Yellow River can be seen as another line of evidence (Stevens et al., 2013). In its upper reaches, the Yellow River flows through several geotectonic units, including the Young Tibetan Fault Block in its source areas upstream of Longyang Gorge (Fig. 1), and the Qilian Mountains downstream of Longyang Gorge (Fig. 1) (Shi et al., 2013). The Young Tibetan Fault Block and the Qilian Orogenic Belt both belong to the Northern Tibetan Plateau, and thus are expected to have similar detrital zircon U-Pb age profiles.

However, the Young Tibetan Fault Block may not supply much sediment to the western Maowusu Sandy Land and the Kubuqi Desert. The annual average sediment load at Tangnaihai station (Fig. 1), located close to Longyang Gorge, is much lower than that of Lanzhou (<20%) station (Zheng and Luo, 1998; Su, 2013; Zheng et al., 2013), indicating that not much sediment from the Young Tibetan Fault Block has been transported to the Ningxia-Inner Mongolian section of the Yellow River, as the data of trace element ratios indicate (Fig. 11e). Compared with aeolian sands of the western Maowusu Sandy Land and the Kubuqi Desert, rocks from the north side of the Bayan Har Mountains (Fig. 1) have much higher Zr/Hf values, while rocks around Tangnaihai station have slightly lower Zr/Hf values. Fluvial sediments of the Yellow River collected near the Tangnaihai station (Fig. 1) have similar trace element ratios with rocks nearby, suggesting a local provenance for the sediments near the station. Both low sediment load and different Zr/Hf values exclude the Young Tibetan Fault Block as key source areas for the aeolian sands in the western Maowusu nor for those in the Kubuqi.

Downstream of Longyang Gorge, the Yellow River flows between the western Qinling Orogenic Belt and the Qilian Orogenic Belt (Shi et al., 2013; Fig. 1). The mean annual sediment load between Longyang Gorge (Fig. 1) and Qingtong Gorge (Fig. 1) along the Yellow River shows a steady increase downstream (Su, 2013; Zheng et al., 2013), indicating that sediments deposited downstream of Qingtong Gorge (Fig. 1) should have their sources mainly from this region. Therefore, the western Qinling Orogenic Belt and the Qilian Orogenic Belt are likely to be the initial source areas of fluvial sediments in Ningxia-Inner Mongolian section of the Yellow River, and ultimately the aeolian sands in the western Maowusu and Kubuqi. Further identification can be reached via comparison of trace elements and REE ratios of aeolian sands and rocks in the potential source areas (Fig. 12). Though much overlap exists between these two potential source areas, most aeolian sand samples fall into the field of Qilian Orogenic Belt while only a sub-set appear in the overlapping shadow, indicating the Qilian Orogenic Belt is the most likely original source area for the aeolian sands in the western Maowusu Sandy Land and the Kubuqi Desert.

5.3. Further implications

Covering 400,000 km^2 areas, the Loess Plateau in the south of Ordos Deserts has the thickest loess in the world (Liu, 1985) (Fig. 1). The provenance of loess in the Loess Plateau has been a key aspect for deciphering palaeoclimatic signals in this terrestrial record. Deserts in the up-wind

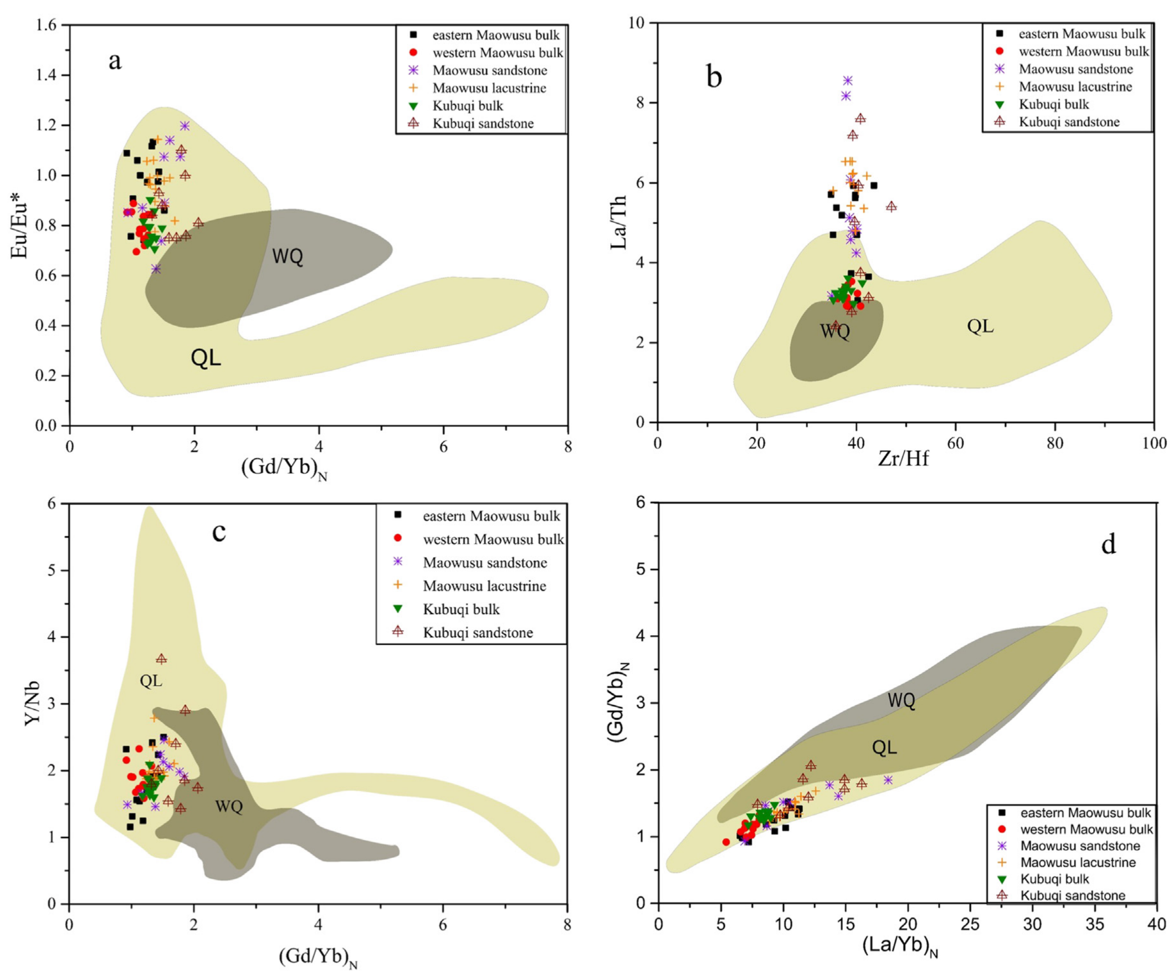

Fig. 12. Bivariate diagrams of trace and rare earth element ratios of samples from the Ordos Deserts, compared with their potential source areas. QL marks the potential source areas of the Qilian Orogenic Belt (Fig. 1) (data from Yan et al., 2010; Tung et al., 2013, 2016; Yu et al., 2013, 2015; Huang et al., 2014); WQ marks the potential source areas of western Qinling Orogenic Belt (Fig. 1) (data from Zhang et al., 2007; Zhu et al., 2011; Liu et al., 2012; Han et al., 2014).

directions in northern and northwestern China, such as the Badain Jaran Desert, the Tengger Desert, and the Ordos Deserts are all potential sources (Fig. 1), but the roles of each desert in providing dust to the Loess Plateau are still a matter of debate (Sun et al., 2007; Yang et al., 2009; Stevens et al., 2013; Che and Li, 2013). Isotopic data suggested that the Alashan Deserts, which include the Badain Jaran Desert, the Tengger Desert, the Wulan Buh Desert (Fig. 1) were the main sources of loess on the Loess Plateau (Sun et al., 2007; Yang et al., 2009). Che and Li (2013) also proposed that dust from the Alashan Deserts could be source of loess of the Loess Plateau based on similar zircon U-Pb age spectra. However, other zircon U-Pb age spectra indicate that loess on the Loess Plateau was mainly derived from the Qaidam Basin and the northern Tibetan Plateau, possibly transported by westerly winds (Pullen et al., 2011). In still other studies, Stevens et al. (2013) suggested that fluvial sediments of the Yellow River, carried from the northern Tibetan Plateau, might be the main provenance of loess on the Loess Plateau.

Recent studies of the Badain Jaran Desert (Fig. 1) show that the aeolian sands there originate mainly from the Qilian Mountains (Fig. 1) (Hu and Yang, 2016). Our study also suggests the Qilian Orogenic Belt as the origin of aeolian sands in the western Maowusu Sandy Land and the Kubuqi Desert, but with fluvial sediments of the Yellow River upwind of these dune fields as the immediate source. As a consequence, the Alashan Deserts, the Ordos Deserts and fluvial sediments of the Yellow River may have similar ultimate source areas because of similar geochemical compositions. Therefore, identification of aeolian sediment sources should not be based solely on geochemistry, but with full attention to geomorphological aspects and wind data.

6. Conclusions

Our major and trace element data of aeolian sands in the Ordos Deserts, supported by our field observations and wind data, enable us to conclude that aeolian sands in the eastern and western Maowusu Sandy Land have different sources. Aeolian sands in the western Maowusu Sandy Land have higher mineralogical maturity, lower Eu/Eu* and La/Th values, compared with those in the eastern Maowusu Sandy Land. Different sources rather than mineralogical separation during wind sorting are interpreted to be the cause of these geochemical differences. Comparison of trace elements and REE ratios of aeolian sediments in the Ordos Deserts with felsic rocks in their potential source areas indicates that aeolian sands in the eastern Maowusu Sandy Land are mainly sourced from the lacustrine sediments and underlying sandstones, while aeolian sands in the western Maowusu and Kubuqi mainly originate from fluvial sediments of the Yellow River in the upwind direction, i.e., the Ningxia-Inner Mongolian section of the river course. Though fine fractions in the aeolian sands of the Maowusu and Kubuqi have obviously negative Eu anomalies compared with bulk sand samples, mineralogical separation during wind sorting rather than different sources are interpreted to be the main reason for this difference. Considering the mean annual sediment loads and trace element ratios, we suggest the Qilian Orogenic Belt is the ultimate source areas of fluvial sediments in the Ningxia-Inner Mongolian section of the Yellow River, and thus the original source of aeolian sands in the western Maowusu Sandy Land and the Kubuqi Desert. Thus, dune fields that are not far apart from one another can have significantly different sediment provenance.

Acknowledgments

We greatly appreciate very valuable comments and suggestions from Editor Andy Plater, Dan Muhs and an anonymous reviewer. To Dan Muhs and Andy Plater we owe tremendous thanks also for having duly corrected and improved the language of the entire manuscript. Our sincere thanks are extended to Prof. Dr. Bernhard Eitel and Prof. Dr. Ulrich Radtke for helpful discussions, and to the National Natural Science Foundation of China (Grant nos.: 41672182; 41430532) and the Alexander von Humboldt Stiftung, Germany (Research Award) for much appreciated support.

References

Amorosi, A., Centineo, M.C., Dinelli, E., Lucchini, F., Tateo, F., 2002. Geochemical and mineralogical variations as indicators of provenance changes in Late Quaternary deposits of SE Po Plain. Sediment. Geol. 15, 273–292.
Blatt, H., Middleton, G., Murray, R., 1972. Origin of Sedimentary Rocks. Prentice-Hall, Inc, Englewood Cliffs, NJ.
Blümel, W.D., 2013. Wüsten. Eugen Ulmer KG, Stuttgart.
Bubenzer, O., Besler, H., Hilgers, A., 2007. Filling the gap: OSL data expanding 14C chronologies of Late Quaternary environmental change in the Libyan Desert. Quat. Int. 175, 41–52.
Bullard, J., McTainsh, G., 2003. Aeolian-fluvial interactions in dryland environments: examples, concepts and Australia case study. Progress in Physical Geography: Earth and Environment. 27, pp. 471–501.
Cameron, K.L., Blatt, H., 1971. Durabilities of sand size schist and 'volcanic' rock fragments during fluvial transport, Elk Creek, Black Hills, South Dakota. J. Sediment. Petrol. 41, 565–576.
Chase, B., 2009. Evaluating the use of dune sediments as a proxy for palaeo-aridity: a southern African case study. Earth Sci. Rev. 93 (1–2), 31–45.
Che, X., Li, G., 2013. Binary sources of loess on the Chinese Loess Plateau revealed by U-Pb ages of zircon. Quat. Res. 80, 545–551.
Cohen, T.J., Nanson, G.C., Larsen, J.R., Jones, B.G., Price, D.M., Coleman, M., Pietsch, T.J., 2010. Late Quaternary aeolian and fluvial interactions on the Cooper Creek Fan and the association between linear and source-bordering dunes, Strzelecki Desert, Australia. Quat. Sci. Rev. 29, 455–471.
Crouvi, O., Schepanski, K., Amit, R., Gillespie, A.R., Enzel, Y., 2012. Multiple dust sources in the Sahara Desert: the importance of sand dunes. Geophys. Res. Lett. 39, 1–8.
Cullers, R.L., 2002. Implications of elemental concentrations for provenance, redox conditions, and metamorphic studies of shales and limestones near Pueblo, CO, USA. Chem. Geol. 191, 305–327.
Dong, Z., Qian, G., Lv, P., Hu, G., 2013. Investigation of the sand sea with the tallest dunes on Earth: China's Badain Jaran Sand Sea. Earth Sci. Rev. 120, 20–39.
Dutta, P.K., Zhou, Z., dos Santos, P.R., 1993. A theoretical study of mineralogical maturation of eolian sand. Geol. Soc. Am. Spec. Pap. 284, 203–209.
Eitel, B., Hecht, S., Mächtle, B., Schukraft, G., Kadereit, A., Wagner, G., Kromer, B., Unkel, I., Reidel, M., 2005. Geoarchaeological evidence from desert loess in the Nazca–Palpa region, southern Peru: palaeoenvironmental changes and their impact on Pre-Columbian cultures. Archaeometry 47, 137–185.
Fang, F., 2010. Approach to a Connection of Geochemical Feature between Source and Sink: Evidence From the Huanghe Drainage [D Referring to Thesis Available Online, Same in Following List]. China University of Geosciences, Beijing (in Chinese with English abstract).
Fryberger, S.G., Dean, G., 1979. Dune forms and wind regime. In: McKee, E.D. (Ed.), A Study of Global Sand Seas, Geological Survey Professional Paper. 1052. U.S. Government Printing Office, Washington.
Garzanti, E., Andò, S., Vezzoli, G., Lustrino, M., Boni, M., Vermeesch, P., 2012. Petrology of the Namib Sand Sea: long-distance transport and compositional variability in the wind-displaced Orange Delta. Earth Sci. Rev. 112, 173–189.
Garzanti, E., Resentini, A., Andò, S., Vezzoli, G., Pereira, A., Vermeesch, P., 2015. Physical controls on sand composition and relative durability of detrital minerals during ultra-long distance littoral and aeolian transport (Namibia and southern Angola). Sedimentology 62, 971–996.
Goudie, A., 2002. Great Warm Deserts of the World: Landscapes and Evolution. Oxford University Press, New York.
Goudie, A., 2009. Dust storms: recent developments. J. Environ. Manag. 90, 89–94.
Han, J., Yao, J., Chen, Y., 2014. Geochronology and geochemistry of the Dashui adakitic granitoids in the western Qinling Orogen, central China: implications for Triassic tectonic setting. Geol. J. 49, 383–401.
Hayes, J.R., 1962. Quartz and feldspar content in South Platte, Platte, and Missouri River sands. J. Sediment. Petrol. 32, 793–800.
Hu, F., Yang, X., 2016. Geochemical and geomorphological evidence for the provenance of aeolian deposits in the Badain Jaran Desert, northwestern China. Quat. Sci. Rev. 131, 179–192.
Huang, H., Niu, Y., Nowell, G., Zhao, Z., Yu, X., Zhu, D., Mo, X., Ding, S., 2014. Geochemical constraints on the petrogenesis of granitoids in the East Kunlun Orogenic belt, northern Tibetan Plateau: implications for continental crust growth through syn-collisional felsic magmatism. Chem. Geol. 370, 1–18.
Lancaster, N., Yang, X., Thomas, D., 2013. Spatial and temporal complexity in Quaternary desert datasets: implications for interpreting past dryland dynamics and understanding potential future changes. Quat. Sci. Rev. 78, 301–302.
Lancaster, N., Baker, S., Bacon, S., McCarley-Holder, G., 2015. Owens Lake dune fields: composition, sources of sand, and transport pathways. Catena 134, 41–49.
Lehmkuhl, F., Grunert, J., Hülle, D., Batkhishig, O., Stauch, G., 2018. Paleolakes in the Gobi region of southern Mongolia. Quat. Sci. Rev. 179, 1–23.
Li, H., Yang, X., 2014. Temperate dryland vegetation changes under a warming climate and strong human intervention - with a particular reference to the district Xilin Gol, Inner Mongolia, China. Catena 119, 9–20.
Li, Z., Liu, X., Dong, Y., Xiao, Z., 2013. Geochemistry and zircon U-Pb age of the Paleoproterozoic syn-collisional granites in Helanshan region and its geological significance. Acta Petrol. Sin. 29 (7), 2405–2415 (in Chinese with English abstract).

Lin, X., 2011. A Synthetic Thought of Provenance Analysis in the Terrigenous Clastic Rock Basin-An Example in the Lower Permian Shanxi Formation, Northern Ordos Basin [D]. Chengdu University of Technology, Chendu (in Chinese with English abstract).
Lin, X., Guo, Y., Hou, S., 2014. Estimation of sediment load of ten tributaries of Yellow River in Inner-Mongolia. J. Sediment. Res. 2, 15–20 (in Chinese with English abstract).
Liu, T., 1985. Loess and the Environment. China Ocean Press, Beijing (in Chinese).
Liu, Z., Yang, X., 2013. Geochemical-geomorphological evidence for the provenance of aeolian sands and sedimentary environments in the Hunshandake Sandy Land, Eastern Inner Mongolia, China. Acta Geol. Sin. 87 (3), 801–840 (English Edition).
Liu, C., Pei, X., Li, Z., Li, R., Pei, L., Gao, J., Wei, F., Wang, Y., Wu, S., Chen, Y., 2012. Geochemical features and tectonic setting of the Neoproterozoic granitic gneiss in Tianshui area on the northern margin of West Qinling. Geol. Bull. China 31 (10), 1588–1601.
Liu, J., Zhang, D., Wei, J., Fu, L., Tan, J., Wang, D., Shi, H., Wang, Y., 2016. Zircon U-Pb age and geochemical characteristics of the Paleoproterozoic S-type granite in the northern part of Helanshan and its geological significance. J. Cent. South Univ. 47 (1), 187–197 (in Chinese with English abstract).
Ma, L., Qi, X., Tang, H., Dai, W., 2004. Geological Atlas of China. Geological Publishing House, Beijing (in Chinese).
Mächtle, B., Unkel, I., Eitel, B., Kromer, B., Schiegl, S., 2010. Molluscs as evidence for a late Pleistocene and early Holocene humid period in the southern coastal desert of Peru (14.5°S). Quat. Res. 73, 39–47.
McLennan, S.M., 1993. Weathering and global denudation. J. Geol. 101, 295–303.
McLennan, S.M., 2001. Relationships between the trace element composition of sedimentary rocks and upper continental crust. Geochem. Geophys. Geosyst. 2, 2000GC000109.
Muhs, D.R., 2004. Mineralogical maturity in dunefields of North America, Africa and Australia. Geomorphology 59, 247–269.
Muhs, D.R., 2017. Evaluation of simple geochemical indicators of aeolian sand provenance: Late Quaternary dune fields of North America revisited. Quat. Sci. Rev. 171, 260–296.
Muhs, D.R., Stafford, T.W., Cowherd, S.D., Mahan, S.A., Kihl, R., Maat, P.B., Bush, C.A., Nehring, J., 1996. Origin of the late Quaternary dune fields of northeastern Colorado. Geomorphology 17, 129–149.
Muhs, D.R., Roskin, J., Tsoar, H., Skipp, G., Budahn, J.R., Sneh, A., Porat, N., Stanley, J.D., Katra, I., Blumberg, D.G., 2013. Origin of the Sinai-Negev erg, Egypt and Israel: mineralogical and geochemical evidence for the importance of the Nile and sea level history. Quat. Sci. Rev. 69, 28–48.
Nanson, G., Price, D., Short, S., 1992. Wetting and drying of Australia over the past 300 ka. Geology 20, 791–794.
Nesbitt, H.W., Young, G.M., 1996. Petrogenesis of sediments in the absence of chemical weathering: effects of abrasion and sorting on bulk composition and mineralogy. Sedimentology 43, 341–358.
Nesbitt, H.W., Young, G.M., McLennan, S.M., Keays, R.R., 1996. Effects of chemical weathering and sorting on the petrogenesis of siliciclastic sediments, with implications for provenance studies. J. Geol. 104, 525–542.
Nesbitt, H.W., Fedo, C.M., Young, G.M., 1997. Quartz and feldspar stability, steady and non-steady-state weathering, and petrogenesis of siliciclastic sands and muds. J. Geol. 105, 173–191.
Pan, B., Pang, H., Zhang, D., Guan, Q., Wang, L., Li, F., Guan, W., Cai, A., Sun, X., 2015. Sediment grain-size characteristics and its source implication in the Ningxia–Inner Mongolia sections on the upper reaches of the Yellow River. Geomorphology 246, 255–262.
Pettijohn, F.J., Potter, P.E., Siever, R., 1972. Sand and Sandstone. Springer-Verlag, New York.
Pittman, E.E., 1969. Destruction of plagioclase twins by stream transport. J. Sediment. Petrol. 39, 1432–1437.
Pullen, A., Kapp, P., McCallister, A.T., Chang, H., Gehrels, G.E., Garzione, C.N., Heermance, R.V., Ding, L., 2011. Qaidam Basin and northern Tibetan Plateau as dust sources for the Chinese Loess Plateau and paleoclimatic implications. Geology 39, 1031–1034.
Ran, L., Wang, S., Fan, X., Min, S., Zhao, J., Zhang, R., Zeng, G., 2009. River channel change at Toudaoguai Section and its response to water and sediment supply of the upper Yellow River. Acta Geograph. Sin. 64 (5), 531–540 (in Chinese with English abstract).
Rao, W., Tan, H., Jiang, S., Chen, J., 2011a. Trace element and REE geochemistry of fine- and coarse-grained sands in the Ordos Deserts and links with sediments in surrounding areas. Chem. Erde 71, 155–170.
Rao, W., Chen, J., Tan, H., Jiang, S., Su, J., 2011b. Sr–Nd isotopic and REE geochemical constraints on the provenance of fine-grained sands in the Ordos Deserts, north-central China. Geomorphology 132, 123–138.
Sepulchre, P., Ramstein, G., Fluteau, F., Schuster, M., Tiercelin, J., Brunet, M., 2006. Tectonic uplift and eastern Africa aridification. Science 313, 1419–1423.
She, Z., Ma, C., Mason, R., Li, J., Wang, G., Lei, Y., 2006. Provenance of the Triassic Songpan–Ganzi flysch, west China. Chem. Geol. 231, 159–175.
Shi, X., Jia, X., Wang, H., Wang, H., 2013. Characteristics of heavy mineral in coarse sediment and its indicative significance in the Ningxia-Inner Mongolia Section of the Yellow River. J. Desert Res. 33 (4), 1000–1008 (in Chinese with English abstract).
Shu, P., Niu, D., Li, B., Wen, X., Si, Y., Guo, Y., Hu, G., 2016. Grain size characteristics of modern dune sand and its significance in the Mu Us Sandy Land, China. J. Desert Res. 36 (1), 158–166 (in Chinese with English abstract).
Singhvi, A.K., Williams, M.A.J., Rajaguru, S.N., Misra, V.N., Chawla, S., Stokes, S., Chauhan, N., Francis, T., Ganjoo, R.K., Humphreys, G.S., 2010. A ~200 ka record of climatic change and dune activity in the Thar Desert, India. Quat. Sci. Rev. 29, 3095–3105.
Stevens, T., Carter, A., Watson, T.P., Vermeesch, P., Andò, S., Bird, A.F., Lu, H., Garzanti, E., Cottam, M.A., Sevastjanova, I., 2013. Genetic linkage between the Yellow River, the Mu Us desert and the Chinese Loess Plateau. Quat. Sci. Rev. 78, 355–368.
Su, X., 2013. Characteristics of Runoff and Sediment Variation in Ningxia-Inner Mongolia Reaches of the Upper Yellow River [D]. North China University of Water Resources and Electric Power, Zhengzhou (in Chinese with English abstract).
Sun, Y., Tada, R., Chen, J., Chen, H., Toyoda, S., Tani, A., Isozaki, Y., Nagashima, K., Hasegawa, H., Ji, J., 2007. Distinguishing the sources of Asian dust based on electron spin resonance signal intensity and crystallinity of quartz. Atmos. Environ. 41, 8537–8548.
Taylor, S., McLennan, S., 1985. The Continental Crust: Its Composition and Evolution. Blackwell Scientific Publications, Oxford.
Thomas, D.S.G., Wiggs, G.F.S., 2008. Aeolian system responses to global change: challenges of scale, process and temporal integration. Earth Surf. Process. Landf. 33, 1396–1418.
Tung, K., Yang, H., Liu, D., Zhang, J., Yang, H., Shau, Y., Tseng, C., 2013. The Neoproterozoic granitoids from the Qilian block, NW China: evidence for a link between the Qilian and South China blocks. Precambrian Res. 235, 163–189.
Tung, K., Yang, H., Yang, H., Smith, A., Liu, D., Zhang, J., Wu, C., Shau, Y., Wen, D., Tseng, C., 2016. Magma sources and petrogenesis of the early–middle Paleozoic backarc granitoids from the central part of the Qilian block, NW China. Gondwana Res. 38, 197–219.
Williams, M., 1994. Some implications of past climatic changes in Australia. Trans. R. Soc. S. Aust. 118, 17–25.
Williams, M., 2014. Climate change in deserts. Cambridge University Press, Cambridge.
Williams, M., 2015. Interactions between fluvial and eolian geomorphic systems and processes: examples from the Sahara and Australia. Catena 134, 4–13.
Wu, B., 2004. Effect of the Ten Major Tributaries in the Inner Mongolia on Runoff and Sediment Load as Well as Sedimentation in the Main Stream of the Yellow River. Yellow River. 36 (10) pp. 5–8 (in Chinese with English abstract).
Yan, G., Tan, L., Xu, B., Mou, B., Shao, H., Chen, T., Tong, Y., Ren, K., Yang, B., 2001. Petrogeochemical characteristics of Indosinian alkaline intrusions in Yinshan Area. Acta Petrol. Mineral. 20 (3), 281–292 (in Chinese with English abstract).
Yan, Z., Xiao, W., Windley, B.F., Wang, Z., Li, J., 2010. Silurian clastic sediments in the North Qilian Shan, NW China: Chemical and isotopic constraints on their forearc provenance with implications for the Paleozoic evolution of the Tibetan Plateau. Sediment. Geol. 231, 98–114.
Yang, X., 1991. Geomorphologische Untersuchungen in Trockenräumen NW Chinas unter besonderer Berücksichtigung von Badanjilin und Takelamagan. Göttinger Geographische Abhandlungen 96, 1–124.
Yang, X., Eitel, B., 2016. Understanding the interactions between climate change, landscape evolution, surface processes and tectonics in the earth system: what can the studies of Chinese deserts contribute? Acta Geol. Sin. 90 (4), 1444–1454.
Yang, X., Liu, T., Xiao, H., 2003. Evolution of megadunes and lakes in the Badain Jaran Desert, Inner Mongolia, China during the last 31,000 years. Quat. Int. 104, 99–112.
Yang, X., Liu, Y., Li, C., Song, Y., Zhu, H., Jin, X., 2007a. Rare earth elements of aeolian deposits in Northern China and their implications for determining the provenance of dust storms in Beijing. Geomorphology 87, 365–377.
Yang, X., Zhu, B., White, P.D., 2007b. Provenance of aeolian sediment in the Taklamakan Desert of western China, inferred from REE and major-elemental data. Quat. Int. 175, 71–85.
Yang, X., Zhang, F., Fu, X., Wang, X., 2008. Oxygen isotopic compositions of quartz in the sand seas and sandy lands of northern China and their implications for understanding the provenances of aeolian sands. Geomorphology 102, 278–285.
Yang, J., Li, G., Dai, Y., Rao, W., Ji, J., 2009. Isotopic evidences for provenances of loess of the Chinese Loess Plateau. Earth Sci. Front. 16 (6), 195–206 (in Chinese with English abstract).
Yang, X., Li, H., Conache, A., 2012. Large-scale controls on the development of sand seas in northern China. Quat. Int. 250, 74–83.
Yang, X., Wang, X., Liu, Z., Li, H., Ren, X., Zhang, D., Ma, Z., Rioual, P., Jin, X., Scuderi, L., 2013. Initiation and variation of the dune fields in semi-arid China – with a special reference to the Hunshandake Sandy Land, Inner Mongolia. Quat. Sci. Rev. 78, 369–380.
Yang, X., Forman, S., Hu, F., Zhang, D., Liu, Z., Li, H., 2016. Initial insights into the age and origin of the Kubuqi sand sea of northern China. Geomorphology 259, 30–39.
Yu, S., Zhang, J., del Real, P.G., Zhao, X., Hou, K., Gong, J., Li, Y., 2013. The Grenvillian orogeny in the Altun–Qilian–North Qaidam mountain belts of northern Tibet Plateau: constraints from geochemical and zircon U–Pb age and Hf isotopic study of magmatic rocks. J. Asian Earth Sci. 73, 372–395.
Yu, S., Zhang, J., Qin, H., Sun, D., Zhao, X., Cong, F., Li, Y., 2015. Petrogenesis of the early Paleozoic low-Mg and high-Mg adakitic rocks in the North Qilian orogenic belt, NW China: implications from crustal thickening to extension thinning. J. Asian Earth Sci. 107, 122–139.
Zhang, H., Jin, L., Zhang, L., Harris, N., Zhou, L., Hu, S., Zhang, B., 2007. Geochemical and Pb-Sr-Nd isotopic compositions of granitoids from western Qinling belt: constraints on basement nature and tectonic affinity. Sci. China Ser. D Earth Sci. 50 (2), 184–196.
Zheng, G., Luo, Y., 1998. The Effect of the Yellow River Upper Reach Reservoir on Flood Control, Ice Prevention and Irrigation of Ningxia River Reach and Corresponding Treatments. Yellow River. 20 (6) pp. 12–13 (in Chinese with English abstract).
Zheng, Y., Shang, H., Tao, H., Peng, H., 2013. Analysis on the Varying Characteristics of Water and Sediment in Tangnaihai to Lanzhou Reach of the Yellow River. Yellow River. 35 (1) pp. 17–18 (35 in Chinese with English abstract).
Zhu, Z., Wu, Z., Liu, S., Di, X., 1980. An Outline of Chinese Deserts. Science Press, Beijing (in Chinese).
Zhu, Z., Chen, Z., Wu, Z., Li, J., Li, B., Wu, G., 1981. Study on the Geomorphology of Wind-drift Sands in the Taklamakan Desert. Science Press, Beijing (in Chinese).
Zhu, L., Zhang, G., Chen, Y., Ding, Z., Guo, B., Wang, F., Lee, B., 2011. Zircon U-Pb ages and geochemistry of the Wenquan Mo-bearing granitioids in West Qinling, China: constraints on the geodynamic setting for the newly discovered Wenquan Mo deposit. Ore Geol. Rev. 39, 46–62.